haematologica
Journal of the Ferrata Storti Foundation

The role of PALLD-STAT3 interaction in megakaryocyte differentiation and thrombocytopenia treatment

by Guoming Li, Haojie Jiang, Lingbin Wang, Tingting Liang, Chen Ding, Mina Yang, Yingzhi Shen, Min Xin, Lin Zhang, Jing Dai, Xueqing Sun, Xuejiao Chen, Junling Liu, and Yanyan Xu

Received: February 7, 2024.
Accepted: May 21, 2024.

Citation: Guoming Li, Haojie Jiang, Lingbin Wang, Tingting Liang, Chen Ding, Mina Yang, Yingzhi Shen, Min Xin, Lin Zhang, Jing Dai, Xueqing Sun, Xuejiao Chen, Junling Liu, and Yanyan Xu. The role of PALLD-STAT3 interaction in megakaryocyte differentiation and thrombocytopenia treatment.
Haematologica. 2024 May 30. doi: 10.3324/haematol.2024.285242 [Epub ahead of print]

The role of PALLD-STAT3 interaction in megakaryocyte differentiation and thrombocytopenia treatment

Guoming Li[1#], Haojie Jiang[1#], Lingbin Wang[1], Tingting Liang[1], Chen Ding[1], Mina Yang[1], Yingzhi Shen[1], Min Xin[2], Lin Zhang[1], Jing Dai[2], Xueqing Sun[1], Xuejiao Chen[3*], Junling Liu[1,4*], Yanyan Xu[1*]

1 Department of Biochemistry and Molecular Cell Biology, Key Laboratory of Cell Differentiation and Apoptosis of Chinese Ministry of Education, Shanghai Jiao Tong University School of Medicine, Shanghai, China.

2 Department of Laboratory Medicine, Ruijin Hospital, Shanghai Jiao Tong University School of Medicine, Shanghai, China.

3 School of Basic Medicine, Hubei University of Arts and Science, Xiangyang, Hubei Province, China.

4 Shanghai Synvida Biotechnology Co., Ltd, Shanghai, China.

Running title: PALLD regulates platelet biogenesis

[*]Correspondence:

Xuejiao Chen, e-mail: ruipiaoc@163.com.

Junling Liu, e-mail: liujl@shsmu.edu.cn.

Yanyan Xu, e-mail: xuyanyan901@163.com.

Data-sharing statement : The data that support the findings of this study are available from the corresponding author (Yanyan Xu, xuyanyan901@163.com) upon reasonable request.

Authorship

Contribution: G.L., Y.X., J.L., H.J. and X.C. designed the experiments, analyzed data, and wrote

the paper; G.L., Y.X. and H.J. performed the experiments; X.C. provided the animal model; L.W., T.L., C.D., M.Y., M.X., Y.S., L.Z. and J.D. helped with the experiments.

Disclosure of Conflicts of Interest

The authors declare no competing financial interests.

Acknowledgments

The authors thank the technical support from the Core Facility of Basic Medical Sciences in Shanghai Jiao Tong University School of Medicine.

Funding

This work was supported by the National Natural Science Foundation of China (82322004, 82170126, 82030004, 31830050, 82200131 and 81970127), the National Key R&D Program of China (2021YFA0804900 and 2023YFC2507800), the Postdoctoral Fellowship Program of CPSF (GZB20230432), the Innovative research team of high-level local universities in Shanghai (SHSMU-ZDCX20211801), and the Bureau of Xiangyang City Science and Technology Project (2022YL02A).

Abstract

Impaired differentiation of megakaryocytes constitutes the principal etiology of thrombocytopenia. The signal transducer and activator of transcription 3 (STAT3) is a crucial transcription factor in regulating megakaryocyte differentiation, yet the precise mechanism of its activation remains unclear. PALLD, an actin-associated protein, has been increasingly recognized for its essential functions in multiple biological processes. This study revealed that megakaryocyte/platelet-specific knockout of PALLD in mice exhibited thrombocytopenia due to diminished platelet biogenesis. In megakaryocytes, PALLD deficiency led to impaired proplatelet formation and polyploidization, ultimately weakening their differentiation for platelet production. Mechanistic studies demonstrated that PALLD bound to STAT3 and interacted with its DNA-binding domain (DBD) and Src homology 2 (SH2) domain via Immunoglobulin domain 3 (Ig3). Moreover, the absence of PALLD attenuated STAT3 Y705 phosphorylation and impeded STAT3 nuclear translocation. Based on the PALLD-STAT3 binding sequence, we designed a peptide C-P3, which can facilitate megakaryocyte differentiation and accelerate platelet production *in vivo*. In conclusion, this study highlights the pivotal role of PALLD in megakaryocyte differentiation and proposes a novel approach for treating thrombocytopenia by targeting the PALLD-STAT3 interaction.

Introduction

Thrombocytopenia presents clinical concern due to its high incidence and potential for severe complications. It is defined by platelet counts falling below 0.15×10^{12}/L, resulting in significant spontaneous bleeding and subcutaneous purpura.[1, 2] Notably, when the platelet counts fall below 0.02×10^{12}/L, patients will face a substantial risk of severe hemorrhagic events, such as traumatic intracranial bleeding and gastrointestinal hemorrhage.[3] Thrombocytopenia has a variety of causes. Impaired differentiation of megakaryocytes, leading to a reduction in platelet counts, constitutes the principal etiology of thrombocytopenia.

Megakaryocytes are derived from hematopoietic stem cells and predominantly reside within the bone marrow.[4, 5] During thrombocytopoiesis, megakaryocytes differentiate through a series of tightly regulated complex processes, including endomitosis, membrane system invagination, and proplatelet formation (PPF).[6, 7] Research into megakaryocytes differentiation enhances our understanding of platelet production, which is critical for managing thrombocytopenia.

TPO/Mpl/JAK2/STAT3 pathway is the principal signaling pathway responsible for regulating megakaryocyte differentiation and platelet production.[8, 9] When thrombopoietin (TPO) binds and activates the myeloproliferative leukemia protein (MPL), the receptor-associated Janus kinase 2 (JAK2) is subsequently phosphorylated, recruiting and phosphorylating the signal transducer and activator of transcription 3 (STAT3).[10-12] STAT3 enters the nucleus and binds to the promoter regions of specific genes, such as MYC and Zinc Finger Protein 460 (ZNF460), through the DNA-binding domain (DBD), thus regulating the expression of such genes.[13, 14] Given STAT3's central role in executing the cellular responses initiated by the pathway, targeting STAT3 may be a key to understanding megakaryocyte differentiation.

PALLD, belonging to the cytoskeletal immunoglobulin domain-containing family, exhibits ubiquitous expression in mammals and localizes to various actin-rich subcellular structures, including stress fibers and focal adhesions.[15-17] Studies recently have shown the critical role of PALLD in various physiological and pathological processes. During the early stages of smooth muscle cell (SMC) differentiation, PALLD interacts with the CArG element within the genome to regulate the expression of smooth muscle actin (SMA) and SM22, thus promoting precursor SMC differentiation.[18] PALLD can also promote cancer stem cell-like properties and tumorigenicity by activating the Wnt/β-catenin signaling pathway.[19] Our previous study reported that PALLD

exhibited abundant expression in platelets and was involved in the activation of platelets.[20] This prompted us to consider whether PALLD had an earlier role in megakaryocytes and potentially in platelet biogenesis.

This study found that the absence of PALLD significantly inhibited megakaryocyte differentiation, leading to thrombocytopenia. PALLD interacts with the SH2 domain and DBD of STAT3 to sustain STAT3 function during megakaryocyte differentiation. By exploiting the binding sequence of PALLD and STAT3, we have developed peptide C-P3 that can enhance STAT3 activation and promote thrombopoiesis *in vivo*. These findings help to reveal the molecular mechanisms underlying megakaryocyte differentiation and provide a promising target for the intervention of thrombocytopenia.

Methods

Mice, antibodies, reagents and more methods

Detailed descriptions of antibodies, reagents, mice and other methods are included in the supplemental materials.

Platelet preparation

Platelets were prepared as described before.[21] Briefly, whole blood (including 1U/mL apyrase and 0.1 μg/mL PGE1) was centrifugated at 200 x g for 10 minutes to obtain platelet-rich plasma (PRP). PRP (including 5 mM EDTA) was centrifugated at 800 x g for 10 minutes to obtain washed platelets. Human platelet preparation and related experiments were approved by the Research Ethics Committee of Shanghai Jiao Tong University College of Basic Medical Sciences.

Flow cytometry and flow sorting

Cells from blood and bone marrow were separated and resuspended in FACS buffer. For reticulated platelets analysis, cells were stained with thiazole orange for 60 minutes. For apoptotic platelets analysis, cells were stained with Annexin V for 10 minutes. Both samples were detected on CytoFLEX (Beckman Coulter). For megakaryocyte sorting, cells were stained with anti-CD41 and anti-CD42b antibodies for 30 minutes, and sorted on FACS Aria II (BD Biosciences).

Platelet lifespan assay

Mice were injected with Sulfo-NHS-LC-Biotin via the tail vein. Platelets from orbital blood were separated and stained with streptavidin. Flow cytometry was used to measure the mean fluorescence intensity of streptavidin in platelets.

Platelet regeneration assay

Mice were injected with anti-CD42b antibody (Emfret) via the tail vein. Platelets from orbital blood were quantified using the XN-1000V automatic modular animal blood and body fluid analyzer (Sysmex).

Megakaryocyte induction and differentiation

Megakaryocytes were prepared as described before.[22] Briefly, fetal livers were obtained from 13.5-day pregnant mice and cultured in Dulbecco's modified medium containing 10 % fetal bovine serum, 1 % penicillin/streptomycin stock solution (10000 U/mL), and 25 IU/mL recombinant human TPO (3SBIO) for four days. Purified megakaryocytes were separated by 3 % BSA and 1.5 % BSA.

Megakaryocyte proplatelet forming (PPF) and ploidy assay

Fetal liver-derived megakaryocytes were cultured on slides coated with fibrinogen (Sigma) for differentiation. Then they were fixed and stained with anti-α-Tubulin antibody, imaged using TCS SP8 X (Leica) or N-SIM (Nikon). For the ploidy assay, megakaryocytes were stained with anti-CD41 antibody and fixed overnight. Then they were incubated with 50 μg/mL propidium iodide, 100 μg/mL RNase A, and 0.2 % Triton X-100 for 30 minutes. Polyploidy was analyzed using flow cytometry.

Enzyme-linked immunosorbent assay (ELISA)

HEK293T cells were transfected with pcDNA3.1-Flag or Flag-STAT3 plasmids for 48 hours. Total protein was collected using lysis buffer and added to wells coated with PALLD peptides. Each well was incubated with anti-Flag antibody (Sigma) for 1 hour at room temperature, followed by horseradish peroxidase (HRP)-conjugated secondary antibody (Jackson ImmunoResearch

Laboratories). 2 M H_2SO_4 was used to terminate the color change. The absorption at 450 nm was measured.

Data analysis

Data analysis for the experiment was conducted using GraphPad Prism 9 software. A significance level of $p \leq 0.05$ was considered to determine statistically significant variations among the values.

Results

PALLD deficiency diminished platelet production in mice.

To investigate the impact of PALLD on platelets and megakaryocytes, we established megakaryocyte/platelet-specific PALLD knockout mice (*pf4-Cre*$^{+}$ *PALLD*$^{f/f}$, *PALLD*$^{-/-}$).[23, 24] As expected, PALLD protein levels were decreased in *PALLD*$^{-/-}$ platelets but remained unchanged in other hemocytes (Figure 1A). Peripheral blood cell analysis revealed significantly reduced platelet counts in the *PALLD*$^{-/-}$ mice ($0.45 \pm 0.02 \times 10^{12}$ platelets/L), compared to the *PALLD*$^{f/f}$ mice ($0.94 \pm 0.05 \times 10^{12}$ platelets/L), while red and white blood cell counts, mean platelet volume (MPV) and platelet distribution width (PDW), dense and alpha granules of platelets remained unaltered, collectively indicating thrombocytopenia in *PALLD*$^{-/-}$ mice (Figure 1B, Figure S1A-B).

Impaired platelet production or excessive platelet clearance can lead to thrombocytopenia.[5, 25] In peripheral blood, the proportion of newly generated platelets (Figure 1C, Figure S1C) of *PALLD*$^{-/-}$ mice ($3.50\% \pm 0.11\%$) was significantly lower than that of *PALLD*$^{f/f}$ mice ($5.74\% \pm 0.13\%$), and the proportion of apoptotic platelets remained unchanged (Figure 1D, Figure S1D). We further measured platelet regeneration and clearance rates *in vivo*. Anti-CD42b monoclonal antibody was used to deplete platelets, and platelet counts measured at different time points showed that platelet regeneration was diminished in *PALLD*$^{-/-}$ mice compared to *PALLD*$^{f/f}$ mice (Figure 1E). After tail intravenous injection of Sulfo-NHS-LC-Biotin, the proportions of biotin-labeled platelets at different time points indicated similar rates of platelet clearance between *PALLD*$^{f/f}$ mice and *PALLD*$^{-/-}$ mice (Figure 1F). These data suggested that PALLD deficiency impaired platelet production, resulting in thrombocytopenia in mice.

PALLD deficiency impaired megakaryocyte differentiation.

To explore the reason for reduced platelet biogenesis in *PALLD*$^{-/-}$ mice, we evaluated the differentiation ability and number of megakaryocytes. Under TPO stimulation, hematopoietic stem cells in the fetal liver differentiate into megakaryocytes and subsequently mature, extending proplatelets.[26, 27] We found that fetal liver-derived *PALLD*$^{-/-}$ megakaryocytes generated fewer proplatelets than *PALLD*$^{-/-}$ megakaryocytes at 6 and 8 hours, with decreased number of proplatelet tips, while the F-actin morphology and tips diameter remained relatively unchanged (Figure 2A-C, Figure S2A-C). The unaltered tip diameter in *PALLD*$^{-/-}$ megakaryocytes is consistent with our observations of unchanged MPV and PDW (Figure S1A). During megakaryocyte differentiation, endomitosis results in accumulated DNA content and the formation of high ploidy in megakaryocytes. *PALLD*$^{-/-}$ megakaryocytes derived from the fetal liver or bone marrow showed a higher proportion of normal ploidy ($\leq$ 4N) and a lower ratio of hyperploid ($\geq$ 8N) (Figure 2D-E). From these data, PALLD deficiency impaired megakaryocyte proplatelet formation and polyploidization.

Immunohistochemistry analysis of major thrombopoiesis organs (bone marrow and spleen) in mice revealed that PALLD deficiency had no effect on the number of megakaryocytes (Figure 3A-B).[28, 29] CFU-MK assay indicated that PALLD deficiency did not impact the ability of bone marrow and fetal liver-derived cells to form colonies (Figure 3C).[30] The plasma TPO remained at a similar level in *PALLD*$^{f/f}$ and *PALLD*$^{-/-}$ mice (Figure 3D). All these data show that PALLD deficiency impaired megakaryocyte differentiation, leading to thrombocytopenia in mice.

PALLD interacted with STAT3 and sustained STAT3 activation in megakaryocyte differentiation.

To understand the molecular mechanism of PALLD's impact on megakaryocyte differentiation, we collected total RNA and PALLD co-immunoprecipitation (Co-IP) proteins from bone marrow-derived megakaryocytes of *PALLD*$^{f/f}$ and *PALLD*$^{-/-}$ mice, and performed Next-generation RNA-Seq and liquid chromatography-mass spectrometry (LC-MS) respectively (Figure 4A).

Differentially expressed genes ($P < 0.05$, $|\log_2 FC| > 1.0$) were clustered, revealing 73 up-regulated and 63 down-regulated genes in *PALLD*$^{-/-}$ megakaryocytes compared to *PALLD*$^{f/f}$ megakaryocytes (Figure 4B, Figure S2D, Table S1-2). Among these, the JAK-STAT pathway showed significant enrichment by gene ontology (GO) analysis (Figure 4C, Table S3). Based on

the mass spectrometry results, we found that PALLD interacted with STAT3. Co-IP experiments in human platelets or HEK293T cells also confirmed that PALLD bound to STAT3 (Figure 4D-E).

STAT3 is a crucial transcription factor in megakaryocyte differentiation, which can be activated by the TPO/Mpl/JAK2 pathway.[22, 31] After treating platelets and megakaryocytes with TPO, we found reduced phosphorylation level of STAT3 Y705 in *PALLD*$^{-/-}$ platelets and megakaryocytes (Figure 4F, Figure S2E). In PPF experiments, nuclear localization of STAT3 decreased in *PALLD*$^{-/-}$ megakaryocytes derived from the fetal liver compared to that of *PALLD*$^{f/f}$ (Figure 4G-H). These findings suggest that PALLD participates in preserving TPO-stimulated STAT3 activation in platelets and megakaryocytes.

PALLD interacted with the DBD and SH2 domain of STAT3 and colocalized with STAT3 in both the nucleus and cytoplasm.

Among the various isoforms of PALLD, the 90 kDa isoform was the most abundant in platelets, while others, such as the 200 kDa isoform or 140 kDa isoform, were nearly unexpressed (Figure S2F).[32] This led us to focus our research on the 90 kDa PALLD isoform.

To explore the precise domains responsible for the PALLD-STAT3 interaction, we designed truncated forms of both proteins based on their fundamental structures and expression stability. The results of Co-IP experiments demonstrated that PALLD interacted with the DNA-binding domain (DBD) and Src homology 2 (SH2) domain of STAT3, and STAT3 interacted with the Immunoglobulin domain 3 (Ig3) of PALLD (Figure 5A-C). Using the protein-protein docking model, we predicted a surface binding model for the interaction between PALLD's Ig3 domain, STAT3's DBD and SH2 domain (Figure 5D).

Under a super-resolution structured illumination microscope (SIM), PALLD colocalized with STAT3 in the cytoplasm and nucleus (Figure 5E). Co-IP results also confirmed PALLD-STAT3 interaction in the cytoplasm and nucleus (Figure S3C-D). Additionally, PALLD and STAT3 showed diminished localization in the nucleus when treated with nuclear import inhibitor Ivermectin (Iver) and accumulated in the nucleus when treated with nuclear export inhibitor Leptomycin B (LMB) (Figure S3A-B).[33-35] All data showed that PALLD colocalized with STAT3 in both the nucleus and cytoplasm.

Most proteins located at the nucleus in eukaryotic cells possess NLSs that can facilitate

protein transport through the nuclear pore complexes (NPC) into the nucleus.[36, 37] We found that PALLD colocalized with NPC, and verified that the KPKK or PKKV sequence may serve as the NLSs for PALLD (Figure S3E-G). Furthermore, through chromatin immunoprecipitation (Ch-IP) and utilizing the STAT3-binding promoter sequence as primers (Figure S3H), PALLD was found to interact with the STAT3 transcription complex and may act as a transcription cofactor of STAT3.[13, 14]

Peptide C-P3 promoted megakaryocyte differentiation and platelet production.

To further clarify the specific binding sequence between PALLD and STAT3, we divided the Ig3 domain of PALLD into seven shorter sequences (1-30, 31-60, 61-74, 75-100, 101-118, 119-145, and 146-162), each comprising 30 or fewer amino acids (Figure 6A). ELISA analysis showed notable interaction between peptide 75-100 and STAT3. Then, we subdivided peptide 75-100 into four shorter sequences (P1, P2, P3, P4) and found that peptide P3 exhibited distinct and specific binding to STAT3 (Figure 6B). P3 weakened the binding of PALLD to the DBD but strengthened the binding to the SH2 domain (Figure 6C). Furthermore, in the protein-protein docking model, P3 probably provided the optimal spatial configuration for the PALLD-STAT3 interaction (Figure 6D).

Cell-penetrating peptides (CPPs) are short peptides that facilitate the entry of biomacromolecules into cells through endocytosis or direct penetration of the cell membrane. To explore the cellular function of P3, we designed peptide C-P3 by fusing a kind of CPP, TAT (GRKKRRQRRR) derived from HIV, to the N terminus of P3 (Figure 7A).[38] IF images showed that C-P3 was successfully internalized and localized in megakaryocytes and platelets (Figure 7B, Figure S4A). In platelets, C-P3 promoted the phosphorylation levels of STAT3 Y705 but had no effect on *PALLD*$^{-/-}$ platelets (Figure 7C). In PPF experiments, C-P3 promoted megakaryocytes extend more and longer proplatelet branches as the concentration increased, culminating in forming a complex network structure (Figure 7D-E, Figure S4D).

To further explore the function of C-P3 *in vivo*, this peptide was injected into the bone marrow of mice. Images and flow cytometry analysis further confirmed the penetration of peptide C-P3 (Figure S4B and S4C). Moreover, C-P3 accelerated the rate of platelet regeneration, resulting in a quicker restoration of platelet levels to the normal range (Figure 7F). These findings provide evidence that C-P3 can activate STAT3 and promote megakaryocyte differentiation and

platelet production (Figure 7G), providing a potential implication for the clinical treatment of thrombocytopenia.

Discussion

In this study, we found that mice lacking PALLD exhibited thrombocytopenia with decreased platelet production and poor PPF formation, indicating the role of PALLD in megakaryocyte differentiation. PALLD binds to STAT3 and sustains activation of STAT3 during megakaryocyte differentiation. Targeting the PALLD-STAT3 interaction may provide a promising target for the intervention of thrombocytopenia.

PALLD was initially characterized independently by two research groups,[16, 17] as a molecular scaffold that regulates the cytoskeleton network. Previous studies have shown that PALLD binds to actin via the Ig3 domain and is localized in various actin-rich subcellular structures, including stress fibers, focal adhesions and Z disks.[15, 39] Recent studies have reported novel roles of PALLD in cell adhesion and motility, contributing to the invasive motility of cancer cells.[40-42] Our former research also suggested that PALLD was involved in platelet activation and arterial thrombosis.[20] This study identified PALLD's role in megakaryocyte differentiation through interacting with STAT3, proposing and elaborating new mechanisms and functions of PALLD.

The TPO/Mpl/JAK2/STAT3 signaling pathway is the major signaling pathway to regulate megakaryocyte differentiation and platelet biogenesis. Once activation, STAT3 is phosphorylated and enters the nucleus to induce transcription of differentiated-related gene.[22, 31] PALLD maintains TPO-induced STAT3 activation in platelets and megakaryocytes. When PALLD deficiency is present, reduced STAT3 activation probably affects the expression of several downstream genes, ultimately leading to impaired megakaryocyte differentiation. For example, Fscn1, a gene involved in actin cytoskeleton dynamics and transcriptionally regulated by STAT3, is significantly down-regulated in *PALLD*$^{-/-}$ megakaryocytes, and its reduced expression has been reported to be associated with decreased proplatelet formation.[43, 44] The downstream molecular mechanism impacted by the PALLD-STAT3 interaction still needs further investigation.

As a pivotal transcription factor, STAT3 regulates several genes in hematopoietic stem and progenitor cells, affecting their function and differentiation.[45] Our study found that PALLD enters the nucleus with nuclear localization signals, colocalizes with STAT3 in the nucleus, and may act

as a transcription cofactor. However, elucidating the precise mechanism of PALLD in STAT3-mediated transcription needs further in-depth exploration.

Beyond megakaryocyte differentiation, the constitutive activation of STAT3 is related to the occurrence of multiple tumors, such as breast and colorectal cancers, which are closely related to unfavorable prognosis.[46] Targeting STAT3 has emerged as a promising therapeutic strategy for cancer therapy and is actively being developed.[47] The SH2 domain of STAT3, which contains three binding pockets (pY705, pY+1, and pY-X), is the critical targeting domain for current drug development.[48, 49] However, the widespread expression of STAT3 in various cells makes the development of its target drugs face possible undesirable side effects, emphasizing the critical need for a comprehensive understanding of the precise mechanism of STAT3.[50, 51] In this study, we identified the precise binding sequence between PALLD and STAT3, and designed a related peptide C-P3, which can impact the PALLD-STAT3 interaction, promoting the activation of STAT3. Therefore, our findings may offer more precise and efficacious targets for the design of STAT3-targeting drugs.

In summary, our study revealed that the PALLD-STAT3 interaction plays a crucial role in regulating megakaryocyte differentiation. By targeting the binding site between PALLD and STAT3, we designed a peptide that effectively ameliorates thrombocytopenia in mice, providing new insights and a potential target for the clinical treatment of thrombocytopenia.

References

1. Stanworth SJ, Shah A. How I use platelet transfusions. Blood. 2022;140(18):1925-1936.

2. Corash L, Chen HY, Levin J, et al. Regulation of thrombopoiesis: effects of the degree of thrombocytopenia on megakaryocyte ploidy and platelet volume. Blood. 1987;70(1):177-185.

3. Thachil J, Warkentin TE. How do we approach thrombocytopenia in critically ill patients?. Br J Haematol. 2017;177(1):27-38.

4. Machlus KR, Italiano JE Jr. The incredible journey: From megakaryocyte development to platelet formation. J Cell Biol. 2013;201(6):785-796.

5. Noetzli LJ, French SL, Machlus KR. New Insights Into the Differentiation of Megakaryocytes From Hematopoietic Progenitors. Arterioscler Thromb Vasc Biol. 2019;39(7):1288-1300.

6. Tilburg J, Becker IC, Italiano JE. Don't you forget about me(gakaryocytes). Blood. 2022;139(22):3245-3254.

7. Bluteau D, Lordier L, Di Stefano A, et al. Regulation of megakaryocyte maturation and platelet formation. J Thromb Haemost. 2009;7 Suppl 1:227-234.

8. Kaushansky K, Lok S, Holly RD, et al. Promotion of megakaryocyte progenitor expansion and differentiation by the c-Mpl ligand thrombopoietin. Nature. 1994;369(6481):568-571.

9. Drachman JG, Sabath DF, Fox NE, Kaushansky K. Thrombopoietin signal transduction in purified murine megakaryocytes. Blood. 1997;89(2):483-492.

10. Johnson DE, O'Keefe RA, Grandis JR. Targeting the IL-6/JAK/STAT3 signalling axis in cancer. Nat Rev Clin Oncol. 2018;15(4):234-248.

11. Kuter DJ. New thrombopoietic growth factors. Blood. 2007;109(11):4607-4616.

12. Gurney AL, Wong SC, Henzel WJ, de Sauvage FJ. Distinct regions of c-Mpl cytoplasmic domain are coupled to the JAK-STAT signal transduction pathway and Shc phosphorylation. Proc Natl Acad Sci U S A. 1995;92(12):5292-5296.

13. Sun L, Yan Y, Lv H, et al. Rapamycin targets STAT3 and impacts c-Myc to suppress tumor growth. Cell Chem Biol. 2022;29(3):373-385.

14. Tripathi SK, Chen Z, Larjo A, et al. Genome-wide Analysis of STAT3-Mediated Transcription during Early Human Th17 Cell Differentiation. Cell Rep. 2017;19(9):1888-1901.

15. Goicoechea SM, Arneman D, Otey CA. The role of palladin in actin organization and cell

motility. Eur J Cell Biol. 2008;87(8-9):517-525.

16. Parast MM, Otey CA. Characterization of palladin, a novel protein localized to stress fibers and cell adhesions. J Cell Biol. 2000;150(3):643-656.

17. Mykkänen OM, Grönholm M, Rönty M, et al. Characterization of human palladin, a microfilament-associated protein. Mol Biol Cell. 2001;12(10):3060-3073.

18. Jin L, Gan Q, Zieba BJ, et al. The actin associated protein palladin is important for the early smooth muscle cell differentiation. PLoS One. 2010;5(9):e12823.

19. Shu X, Chen M, Liu SY, et al. Palladin promotes cancer stem cell-like properties in lung cancer by activating Wnt/B-Catenin signaling. Cancer Med. 2023;12(4):4510-4520.

20. Chen X, Fan X, Tan J, et al. Palladin is involved in platelet activation and arterial thrombosis. Thromb Res. 2017;149:1-8.

21. Xu Y, Ouyang X, Yan L, et al. Sin1 (Stress-Activated Protein Kinase-Interacting Protein) Regulates Ischemia-Induced Microthrombosis Through Integrin αIIbβ3-Mediated Outside-In Signaling and Hypoxia Responses in Platelets. Arterioscler Thromb Vasc Biol. 2018;38(12):2793-2805.

22. Jiang H, Yu Z, Ding N, et al. The role of AGK in thrombocytopoiesis and possible therapeutic strategies. Blood. 2020;136(1):119-129.

23. Tiedt R, Schomber T, Hao-Shen H, Skoda RC. Pf4-Cre transgenic mice allow the generation of lineage-restricted gene knockouts for studying megakaryocyte and platelet function in vivo. Blood. 2007;109(4):1503-1506.

24. Skarnes WC, Rosen B, West AP, et al. A conditional knockout resource for the genome-wide study of mouse gene function. Nature. 2011;474(7351):337-342.

25. Kaushansky K. Thrombopoiesis. Semin Hematol. 2015;52(1):4-11.

26. Pang L, Xue HH, Szalai G, et al. Maturation stage-specific regulation of megakaryopoiesis by pointed-domain Ets proteins. Blood. 2006;108(7):2198-2206.

27. Vijey P, Posorske B, Machlus KR. In vitro culture of murine megakaryocytes from fetal liver-derived hematopoietic stem cells. Platelets. 2018;29(6):583-588.

28. Bush LM, Healy CP, Marvin JE, Deans TL. High-throughput enrichment and isolation of megakaryocyte progenitor cells from the mouse bone marrow. Sci Rep. 2021;11(1):8268.

29. Patel SR, Hartwig JH, Italiano JE Jr. The biogenesis of platelets from megakaryocyte

proplatelets. J Clin Invest. 2005;115(12):3348-3354.

30. Yamamoto R, Morita Y, Ooehara J, et al. Clonal analysis unveils self-renewing lineage-restricted progenitors generated directly from hematopoietic stem cells. Cell. 2013;154(5):1112-1126.

31. Plo I, Bellanné-Chantelot C, Mosca M, et al. Genetic Alterations of the Thrombopoietin/MPL/JAK2 Axis Impacting Megakaryopoiesis. Front Endocrinol (Lausanne). 2017;8:234.

32. Rachlin AS, Otey CA. Identification of palladin isoforms and characterization of an isoform-specific interaction between Lasp-1 and palladin. J Cell Sci. 2006;119(Pt 6):995-1004.

33. Wagstaff KM, Sivakumaran H, Heaton SM, Harrich D, Jans DA. Ivermectin is a specific inhibitor of importin α/β-mediated nuclear import able to inhibit replication of HIV-1 and dengue virus. Biochem J. 2012;443(3):851-856.

34. Fung HY, Chook YM. Atomic basis of CRM1-cargo recognition, release and inhibition. Semin Cancer Biol. 2014;27:52-61.

35. Jans DA, Martin AJ, Wagstaff KM. Inhibitors of nuclear transport. Curr Opin Cell Biol. 2019;58:50-60.

36. Kalderon D, Roberts BL, Richardson WD, Smith AE. A short amino acid sequence able to specify nuclear location. Cell. 1984;39(3 Pt 2):499-509.

37. Lu J, Wu T, Zhang B, et al. Types of nuclear localization signals and mechanisms of protein import into the nucleus. Cell Commun Signal. 2021;19(1):60.

38. Copolovici DM, Langel K, Eriste E, Langel Ü. Cell-penetrating peptides: design, synthesis, and applications. ACS Nano. 2014;8(3):1972-1994.

39. Albraiki S, Ajiboye O, Sargent R, Beck MR. Functional comparison of full-length palladin to isolated actin binding domain. Protein Sci. 2023;32(5):e4638.

40. Gilam A, Conde J, Weissglas-Volkov D, et al. Local microRNA delivery targets Palladin and prevents metastatic breast cancer. Nat Commun. 2016;7:12868.

41. Chin YR, Toker A. The actin-bundling protein palladin is an Akt1-specific substrate that regulates breast cancer cell migration. Mol Cell. 2010;38(3):333-344.

42. Wang W, Goswami S, Lapidus K, et al. Identification and testing of a gene expression signature of invasive carcinoma cells within primary mammary tumors. Cancer Res.

2004;64(23):8585-8594. 43. Liu H, Zhang Y, Li L, et al. Fascin actin-bundling protein 1 in human cancer: promising biomarker or therapeutic target?. Mol Ther Oncolytics. 2021;20:240-264.

44. Mazzi S, Dessen P, Vieira M, et al. Dual role of EZH2 in megakaryocyte differentiation. Blood. 2021;138(17):1603-1614.

45. Hillmer EJ, Zhang H, Li HS, Watowich SS. STAT3 signaling in immunity. Cytokine Growth Factor Rev. 2016;31:1-15.

46. Yu H, Pardoll D, Jove R. STATs in cancer inflammation and immunity: a leading role for STAT3. Nat Rev Cancer. 2009;9(11):798-809.

47. Zou S, Tong Q, Liu B, et al. Targeting STAT3 in Cancer Immunotherapy. Mol Cancer. 2020;19(1):145.

48. Kraskouskaya D, Duodu E, Arpin CC, Gunning PT. Progress towards the development of SH2 domain inhibitors. Chem Soc Rev. 2013;42(8):3337-3370.

49. Furtek SL, Backos DS, Matheson CJ, Reigan P. Strategies and Approaches of Targeting STAT3 for Cancer Treatment. ACS Chem Biol. 2016;11(2):308-318.

50. Beebe JD, Liu JY, Zhang JT. Two decades of research in discovery of anticancer drugs targeting STAT3, how close are we?. Pharmacol Ther. 2018;191:74-91.

51. Wong ALA, Hirpara JL, Pervaiz S, et al. Do STAT3 inhibitors have potential in the future for cancer therapy?. Expert Opin Investig Drugs. 2017;26(8):883-887.

Figure legend

Figure 1. Impaired platelet biogenesis leads to thrombocytopenia in *PALLD*$^{-/-}$ mice.

(A) Western blot analysis of PALLD expression in platelets, red blood cells (RBC) and white blood cells (WBC) of *PALLD*$^{f/f}$ and *PALLD*$^{-/-}$ mice.

(B) Platelet, RBC and WBC counts in *PALLD*$^{f/f}$ and *PALLD*$^{-/-}$ mice (n=7, ***P<0.001; ns, not significant).

(C) Representative gating strategy of thiazole orange-stained cells and percentage of reticulated platelets in *PALLD*$^{f/f}$ and *PALLD*$^{-/-}$ mice (n=4, **P<0.01).

(D) Representative gating strategy of annexin V-stained cells and percentage of apoptotic platelets in *PALLD*$^{f/f}$ and *PALLD*$^{-/-}$ mice (n=4).

(E) Platelet counts at different time points after tail intravenous injection of anti-CD42b antibody (2 μg/g) (n=4, *P<0.05, **P<0.01, ***P<0.001).

(F) Biotin-labeled platelets in mice at different time points after tail intravenous injection of Sulfo-NHS-LC-Biotin (n=4).

Figure 2. PALLD deficiency impairs megakaryocyte proplatelet formation and polyploidization.

(A) Immunofluorescence (IF) images of proplatelet-forming (PPF) megakaryocytes derived from the fetal liver of *PALLD*$^{f/f}$ and *PALLD*$^{-/-}$ mice, stained with α-tubulin (Alexa Fluor 488), F-actin (Rhodamine). The scale bars represent 30 μm.

(B) Quantitative analysis of the ratio of PPF-megakaryocytes to total megakaryocytes (6H, n=5, *P<0.05; 8H, n=5, **P<0.01).

(C) Number of proplatelet tips generated by *PALLD*$^{f/f}$ and *PALLD*$^{-/-}$ megakaryocytes (6H, n=5, ***P<0.001; 8H, n=5).

(D) Representative gating strategy for propidium iodide staining of megakaryocytes from fetal liver and bone marrow in *PALLD*$^{f/f}$ and *PALLD*$^{-/-}$ mice. FL-MK, megakaryocytes from fetal liver. BM-MK, megakaryocytes from bone marrow.

(E) Quantitative analysis of the polyploidy ratio in megakaryocytes from fetal liver and bone marrow of *PALLD*$^{f/f}$ and *PALLD*$^{-/-}$ mice (n=4, ***P<0.001).

Figure 3. PALLD deficiency has no effect on megakaryocyte number and colony formation.

(A) Immunohistochemistry images of megakaryocytes in the femur and spleen of *PALLD*$^{f/f}$ and *PALLD*$^{-/-}$ mice. The scale bars represent 30 μm.

(B) Quantitative analysis of megakaryocyte counts in the femur (n=7) and spleen (n=15) sections from *PALLD*$^{f/f}$ and *PALLD*$^{-/-}$ mice.

(C) Colony-forming unit megakaryocyte (CFU-MK) assay of bone marrow and fetal liver-derived cells from *PALLD*$^{f/f}$ and *PALLD*$^{-/-}$ mice (n=5).

(D) Plasma TPO levels in *PALLD*$^{f/f}$ and *PALLD*$^{-/-}$ mice (n=7).

Figure 4. PALLD maintains TPO-induced STAT3 activation in platelets and megakaryocytes.

(A) Schematic diagram of RNA-seq and liquid chromatography-mass spectrometry (LC-MS) of bone marrow-derived megakaryocytes.

(B) Volcano plot of global gene expression profiles in bone marrow megakaryocytes from *PALLD*$^{f/f}$ and *PALLD*$^{-/-}$ mice. Kolmogorov-Smirnov (K-S) test was used for testing the correlation. Down-regulated genes are shown in blue and up-regulated genes are in red.

(C) Gene Ontology (GO) enrichment analysis of functional categories among down-regulated genes in the *PALLD*$^{-/-}$ megakaryocytes. The bar chart represents the enriched GO terms, and the color indicates the significance level.

(D) Co-immunoprecipitation (Co-IP) of human platelet lysates using anti-PALLD and anti-STAT3 antibodies.

(E) Co-IP of lysates from HEK293T cells transfected with Flag-STAT3 and Ha-PALLD.

(F) Western blot of the phosphorylation level of STAT3 Y705 in platelets treated with 25 IU/ml TPO.

(G-H) IF images of undifferentiated and differentiated megakaryocytes derived from the fetal livers of *PALLD*$^{f/f}$ and *PALLD*$^{-/-}$ mice. Stained for α-tubulin (Alexa Fluor 488) and STAT3 (Rhodamine). Statistical results of STAT3 localization are presented (n=5; $^{***}P<0.001$). The scale bars represent 10 μm or 2 μm.

Figure 5. The Ig3 domain of PALLD binds to the DNA-binding domain (DBD) and Src homology 2 (SH2) domain of STAT3 in both the nucleus and cytoplasm.

(A-C) Co-IP of lysates from HEK293T cells transfected with the truncated forms of STAT3 or PALLD. PRR, proline rich region. NTD, N-terminal domain. C-C, coiled-coil domain. TAD, transactivation domain.

(D) Surface binding model of PALLD's Ig3 domain with STAT3's DBD and SH2 domain.

(E) IF images of endogenous PALLD (Alexa Fluor 488) and STAT3 (Rhodamine) in megakaryocytes derived from fetal liver. The 3D-volume rendering of PALLD and STAT3 signals was performed using Imaris software. The scale bars represent 5 μm or 300 nm.

Figure 6. Peptide P3 impacts the interaction between PALLD and STAT3.

(A) Binding affinity of seven PALLD6 peptides to STAT3 detected by Enzyme-linked immunosorbent assay (ELISA). Sequence and statistical analysis from four independent experiments are shown. (***P<0.001)

(B) Binding affinity of four 75-100 peptides to STAT3 detected by ELISA. Sequence and statistical analysis of four independent experiments is shown (***P<0.001).

(C) Co-IP of lysates from HEK293T cells transfected with Flag-PALLD6 and either Ha-STAT3-8 or Ha-STAT3-9, with or without P3.

(D) The binding model of PALLD's Ig3 domain interacting with STAT3's DBD and SH2 domain.

Figure 7. Peptide C-P3 promotes megakaryocyte differentiation and platelet production.

(A) Sequences of peptide C-P3 fused to N-terminal cell-penetrating peptide (CPP).

(B) IF images of α-tubulin (Rhodamine) in megakaryocytes treated with FITC-labeled C-P3. The scale bars represent 5 μm.

(C) Western blot analysis of STAT3 phosphorylation level in *PALLD*$^{f/f}$ and *PALLD*$^{-/-}$ platelets incubated with 0.9% NaCl or C-P3.

(D) IF images of fetal liver-derived megakaryocytes stimulated with PBS or 1 μM and 10 μM C-P3. Stained for α-tubulin (Alexa Fluor 488) and F-actin (Alexa Fluor 647). The scale bars represent 30 μm.

(E) Quantitative analysis of the ratio of PPF-megakaryocytes to total megakaryocytes (n=6, *P<0.05, **P<0.01, ***P<0.001).

(F) Platelets of *PALLD*$^{f/f}$ and *PALLD*$^{-/-}$ mice were eliminated by tail IV injection of anti-CD42b

antibody (2 μg/g). After 36 hours, a bone marrow injection of C-P3 (20 μg/g) was performed. Platelet counts were measured at various time intervals (n=4, $^{*}P<0.05$, $^{**}P<0.01$, $^{***}P<0.001$).

(G) Schematic diagram of peptide C-P3-induced enhancement of megakaryocyte differentiation.

Figure 1

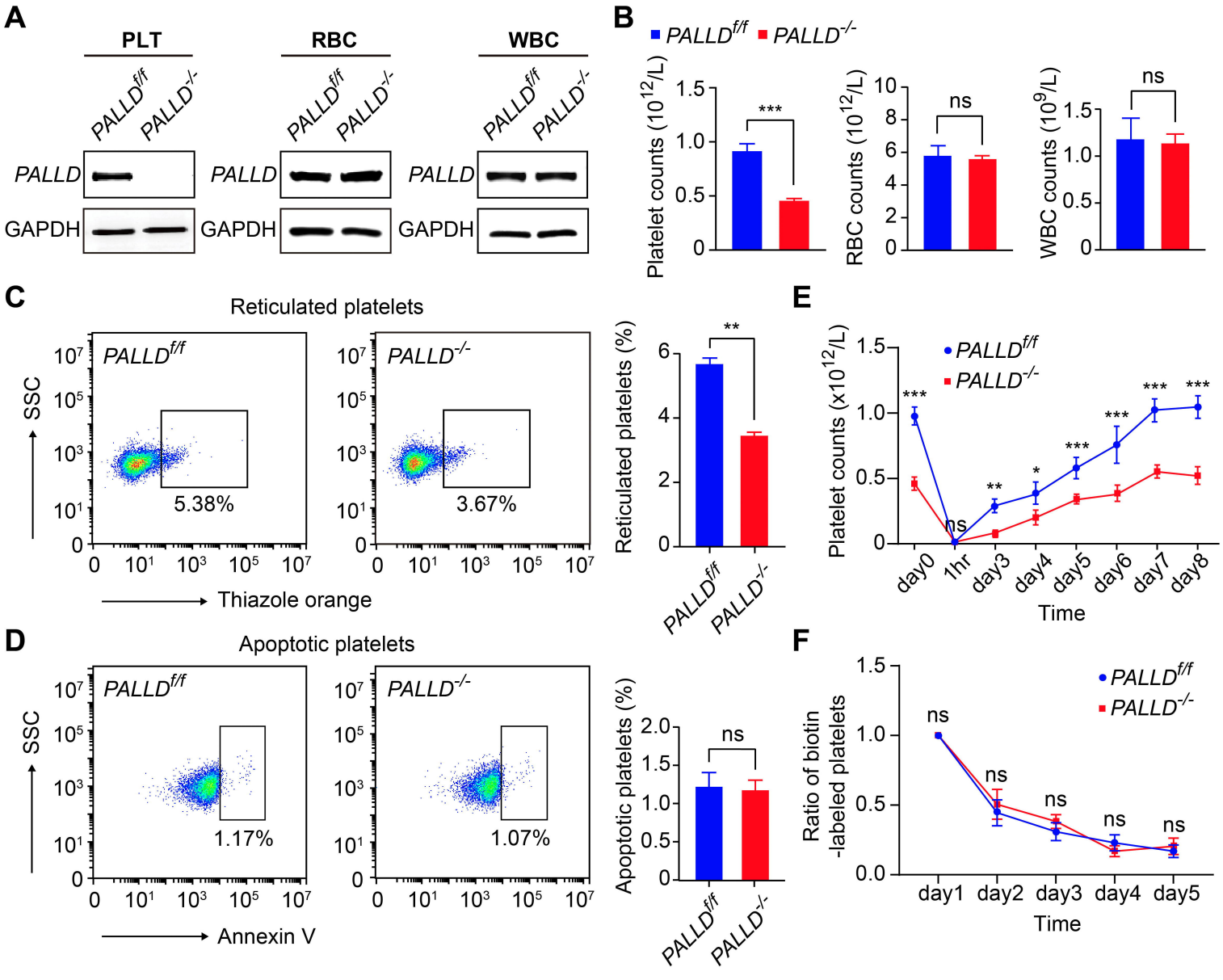
A
PLT
RBC
WBC
PALLD^f/f
PALLD^-/-
PALLD
GAPDH
B
PALLD^f/f
PALLD^-/-
Platelet counts (10^12/L)
RBC counts (10^12/L)
WBC counts (10^9/L)
***
ns
C
Reticulated platelets
SSC
Thiazole orange
5.38%
3.67%
Reticulated platelets (%)
**
D
Apoptotic platelets
Annexin V
1.17%
1.07%
Apoptotic platelets (%)
E
Platelet counts (x10^12/L)
day0
1hr
day3
day4
day5
day6
day7
day8
Time
F
Ratio of biotin -labeled platelets
day1
day2
day3
day4
day5
Time

Figure 2

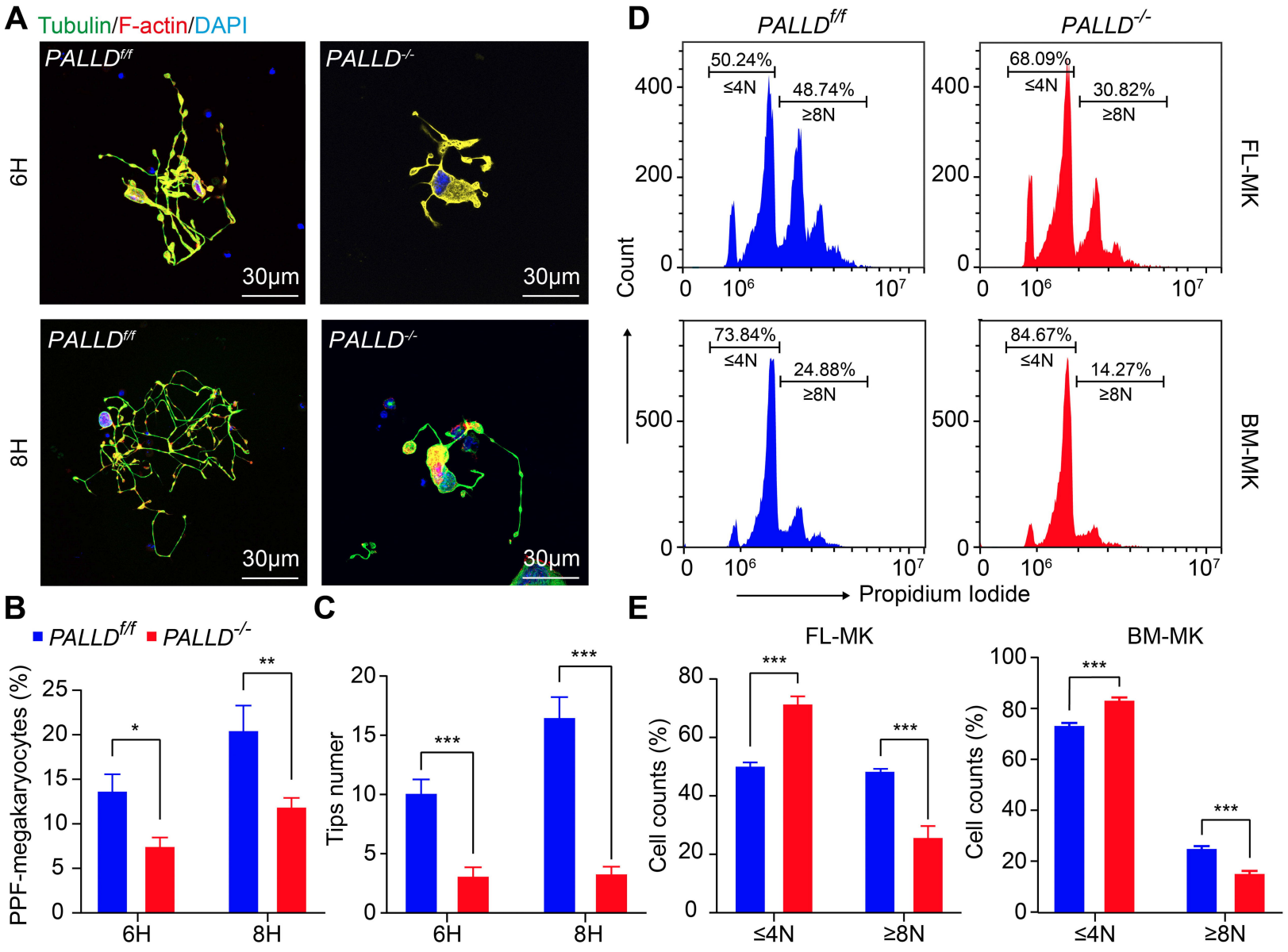
A
Tubulin/F-actin/DAPI
PALLD f/f
PALLD -/-
6H
8H
30μm
D
PALLD f/f
PALLD -/-
50.24%
≤4N
48.74%
≥8N
68.09%
30.82%
73.84%
24.88%
84.67%
14.27%
FL-MK
BM-MK
Count
Propidium Iodide
B
PPF-megakaryocytes (%)
C
Tips numer
E
FL-MK
BM-MK
Cell counts (%)

Figure 3

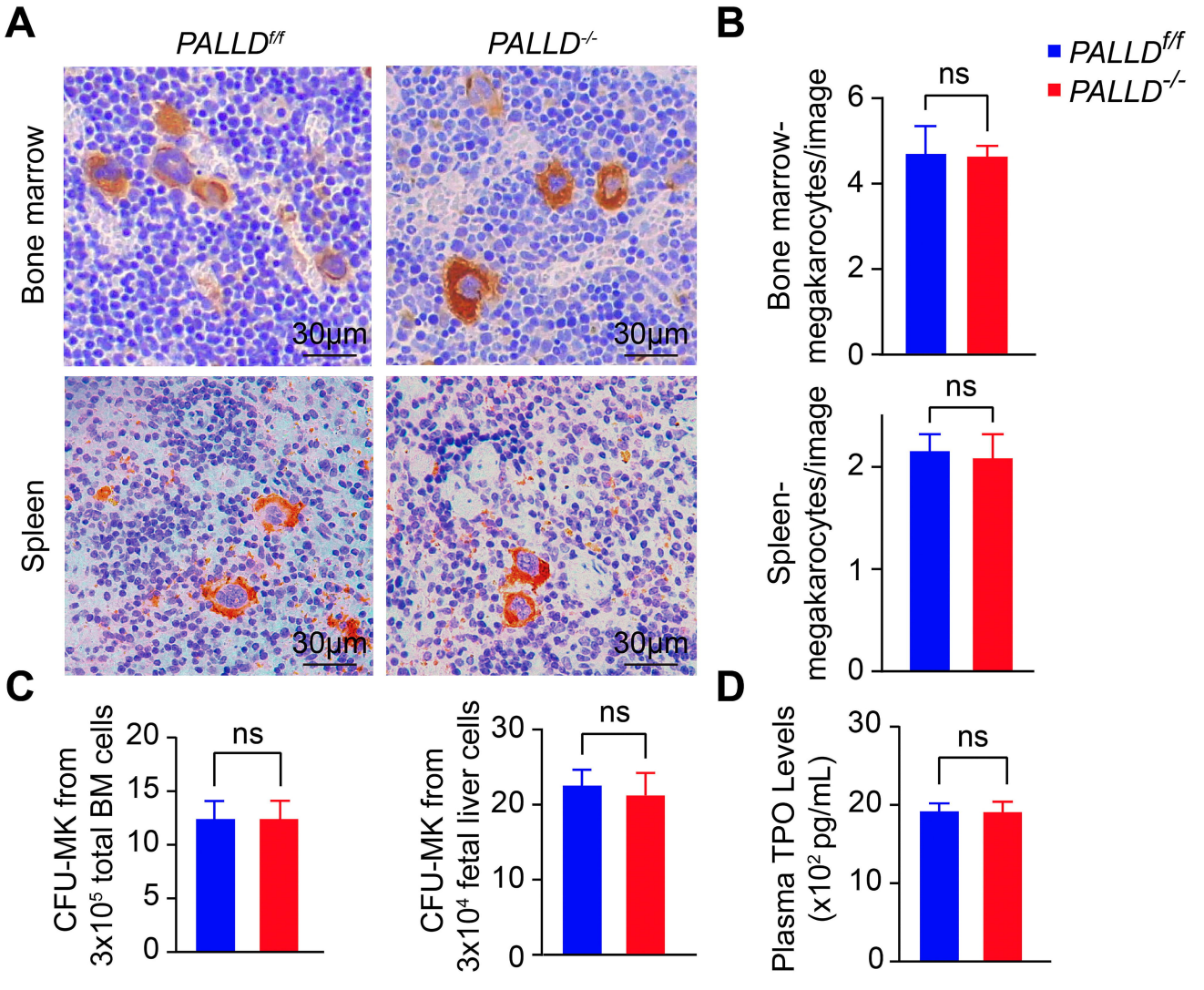
A
PALLD f/f
PALLD -/-
Bone marrow
Spleen
30μm
30μm
30μm
30μm
B
PALLD f/f
PALLD -/-
Bone marrow-megakarocytes/image
ns
0
2
4
6
Spleen-megakarocytes/image
ns
0
1
2
C
CFU-MK from 3x10^5 total BM cells
ns
0
5
10
15
20
CFU-MK from 3x10^4 fetal liver cells
ns
0
10
20
30
D
Plasma TPO Levels (x10^2 pg/mL)
ns
0
10
20
30

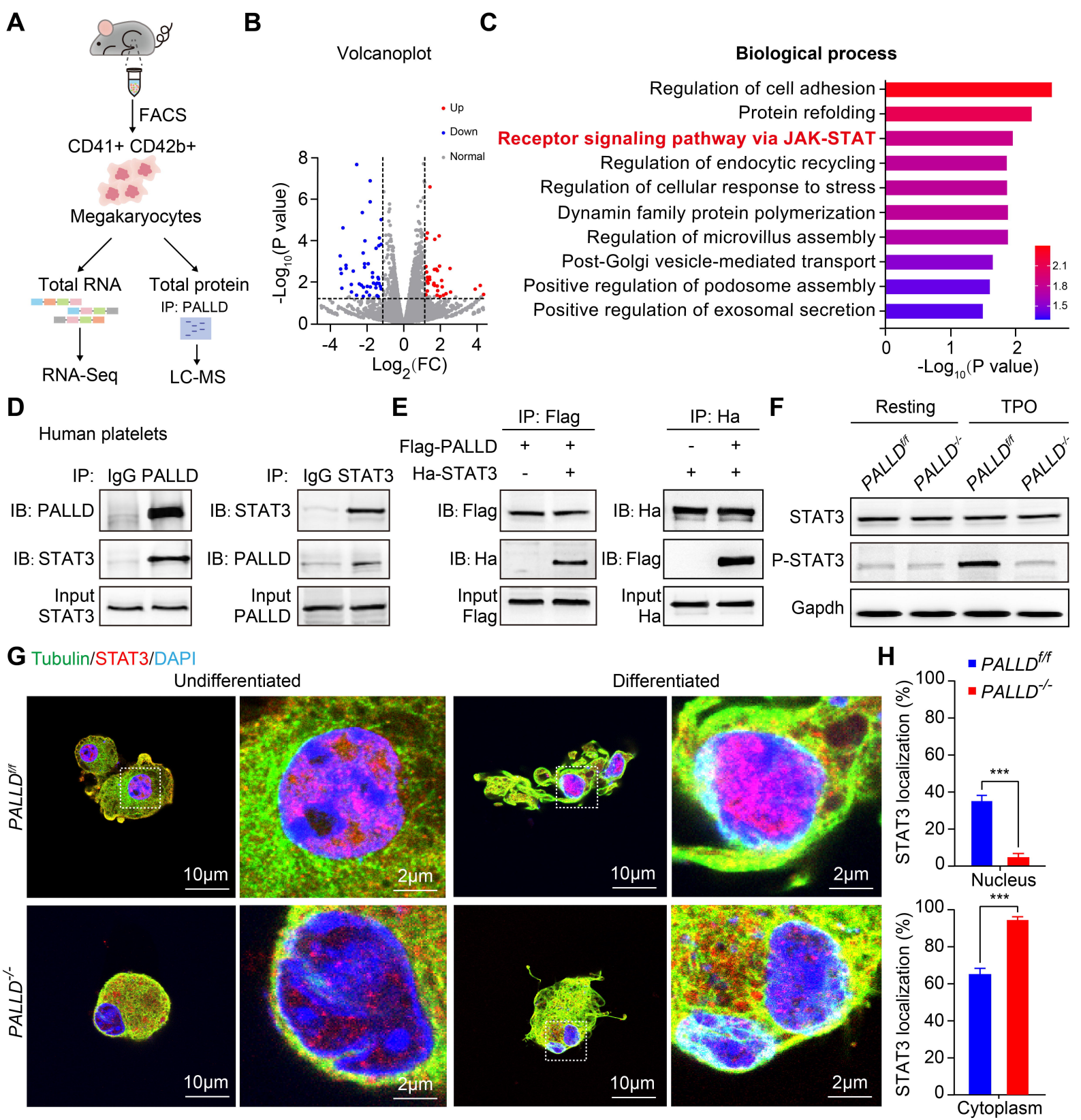
A
FACS
CD41+ CD42b+
Megakaryocytes
Total RNA
Total protein
IP: PALLD
RNA-Seq
LC-MS
B
Volcanoplot
Up
Down
Normal
-Log10(P value)
Log2(FC)
C
Biological process
Regulation of cell adhesion
Protein refolding
Receptor signaling pathway via JAK-STAT
Regulation of endocytic recycling
Regulation of cellular response to stress
Dynamin family protein polymerization
Regulation of microvillus assembly
Post-Golgi vesicle-mediated transport
Positive regulation of podosome assembly
Positive regulation of exosomal secretion
-Log10(P value)
D
Human platelets
IP: IgG PALLD
IP: IgG STAT3
IB: PALLD
IB: STAT3
IB: STAT3
IB: PALLD
Input STAT3
Input PALLD
E
IP: Flag
IP: Ha
Flag-PALLD
Ha-STAT3
IB: Flag
IB: Ha
IB: Ha
IB: Flag
Input Flag
Input Ha
F
Resting
TPO
PALLDf/f
PALLD-/-
STAT3
P-STAT3
Gapdh
G Tubulin/STAT3/DAPI
Undifferentiated
Differentiated
PALLDf/f
PALLD-/-
10μm
2μm
H
PALLDf/f
PALLD-/-
STAT3 localization (%)
***
Nucleus
Cytoplasm

Figure 4

Figure 5

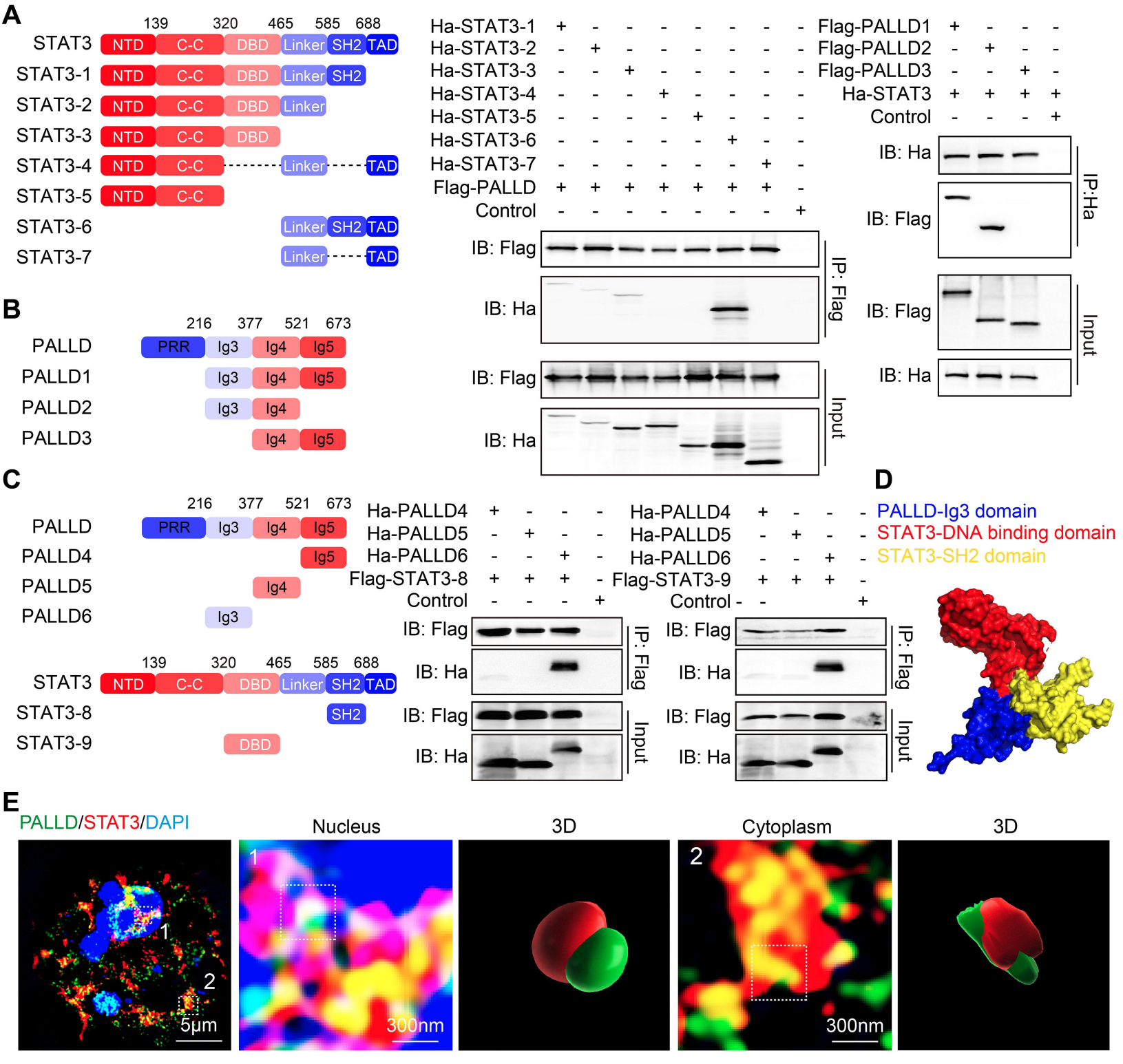
A
139
320
465
585
688
STAT3
NTD
C-C
DBD
Linker
SH2
TAD
STAT3-1
STAT3-2
STAT3-3
STAT3-4
STAT3-5
STAT3-6
STAT3-7
Ha-STAT3-1
Ha-STAT3-2
Ha-STAT3-3
Ha-STAT3-4
Ha-STAT3-5
Ha-STAT3-6
Ha-STAT3-7
Flag-PALLD
Control
IB: Flag
IB: Ha
IP: Flag
Input
Flag-PALLD1
Flag-PALLD2
Flag-PALLD3
Ha-STAT3
IP:Ha
B
216
377
521
673
PALLD
PRR
Ig3
Ig4
Ig5
PALLD1
PALLD2
PALLD3
C
PALLD4
PALLD5
PALLD6
STAT3-8
STAT3-9
D
PALLD-Ig3 domain
STAT3-DNA binding domain
STAT3-SH2 domain
E
PALLD/STAT3/DAPI
Nucleus
3D
Cytoplasm
5μm
300nm

Figure 6

A

PALLD6 peptide sequence

1-30	TYEERMARRLLGADSATVFNIQEPEEETAN
31-60	QEYKVSSCEQRLISEIEYRLERSPVDESGD
61-74	EVQYGDVPVENGMA
75-100	PFFEMKLKHYKIFEGMPVTFTCRVAG
101-118	NPKPKIYWFKDGKQISPKSDHYTIQRDL
119-145	DGTCSLHTTASTLDDDGNYTIMAANPQ
146-162	GRISCTGRLMVQAVNQR

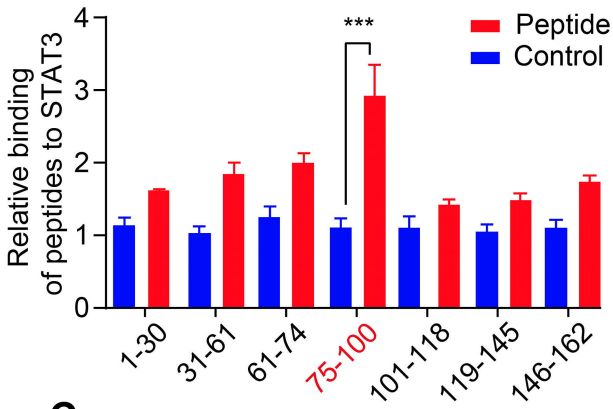

B

75-100 peptide sequence

P1	PFFEMK
P2	LKHYKIFE
P3	GMPVTFTCRVAG
P4	PFFEMKLKHYKIFE

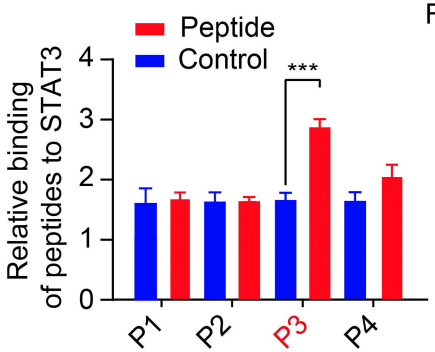

C

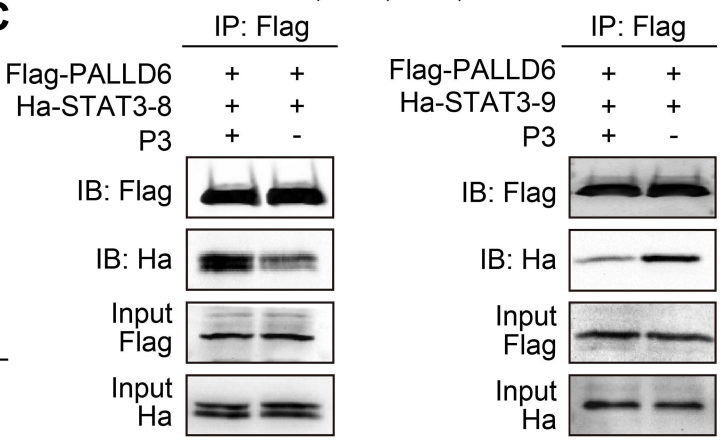

D

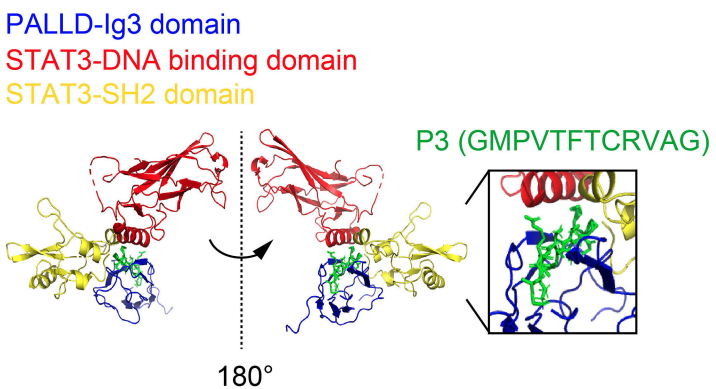

Figure 7

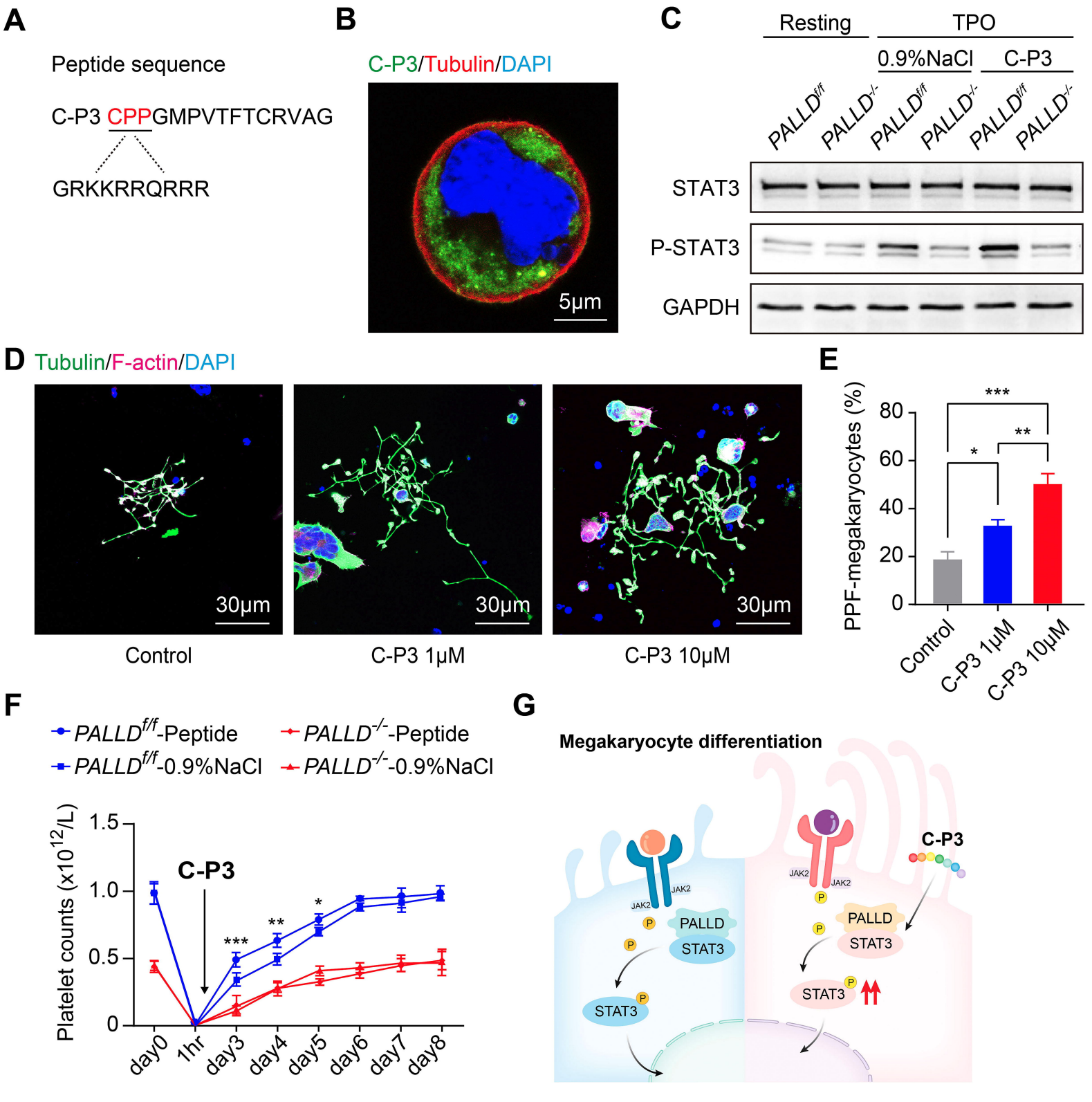
A
Peptide sequence
C-P3 CPPGMPVTFTCRVAG
GRKKRRQRRR
B
C-P3/Tubulin/DAPI
5μm
C
Resting
TPO
0.9%NaCl
C-P3
PALLD f/f
PALLD -/-
PALLD f/f
PALLD -/-
PALLD f/f
PALLD -/-
STAT3
P-STAT3
GAPDH
D
Tubulin/F-actin/DAPI
30μm
30μm
30μm
Control
C-P3 1μM
C-P3 10μM
E
PPF-megakaryocytes (%)
0
20
40
60
80
*
**
***
Control
C-P3 1μM
C-P3 10μM
F
PALLD f/f-Peptide
PALLD -/--Peptide
PALLD f/f-0.9%NaCl
PALLD -/--0.9%NaCl
Platelet counts (x10 12/L)
0
0.5
1.0
1.5
C-P3
***
**
*
day0
1hr
day3
day4
day5
day6
day7
day8
G
Megakaryocyte differentiation
JAK2
JAK2
JAK2
P
PALLD
STAT3
STAT3
C-P3
JAK2
JAK2
P
PALLD
STAT3
STAT3

Supplemental Data

Supplemental Materials and Methods

Mice

The mice were generated by Shanghai Model Organisms Center, Inc. (Shanghai, China), with loxP sites flanking the PALLD exon12 on a C57BL/6 genetic background. They were crossed with *Platelet factor 4* (*Pf4*)-Cre mice (The Jackson Laboratory, 008535, C57BL/6) to produce megakaryocyte/platelet-specific PALLD-deficient mice (*pf4-Cre*$^{+}$ *PALLD*$^{f/f}$, *PALLD*$^{-/-}$).[1,2] All knockout mouse lines were maintained on the C57BL/6 background and genotyped by polymerase chain reaction (PCR). The PCR primers for genotyping the *PALLD-floxed* mice were 5'-AGGCAAGCACTCTACCGACTA-3' and 5'-TAAATGCCACAGACAGAAACTACC-3'. The PCR primers for genotyping the *Pf4-Cre* mice were 5'-GGATAGCGGCAATTACAGAACACC-3' and 5'-AGAACAGGACTCAGCCGTAGCAG-3'. Shanghai Jiao Tong University School of Medicine Animal Care and Use Committee approved the animal research.

Antibodies and reagents

Anti-PALLD polyclonal antibodies, anti-GAPDH polyclonal antibodies and anti-STAT3 polyclonal antibodies were purchased from Proteintech (Wuhan, Hubei, CN). PE-conjugated anti-CD41 monoclonal antibody and APC-streptavidin were purchased from BD Biosciences (San Jose, CA, USA). Anti-HA agarose and EZ-Link (tm) Sulfo-NHS-LC-Biotin were purchased from Pierce (Rockford, IL, USA). Anti-CD42c polyclonal antibodies were purchased from LifeSpan BioSciences, Inc. (Seattle, WA, USA). Anti-CD42b monoclonal antibody was purchased from Emfret Analytics (Würzburg, Germany). Apyrase, PGE1, anti-FLAG M2 affinity gel, anti-FLAG M2 monoclonal antibody, anti-α-Tubulin monoclonal antibody, fibrinogen from human plasma, Leptomycin B solution from *Streptomyces* sp. and Ivermectin were purchased from Sigma-Aldrich (St Louis, MO, USA). Anti-Phospho-STAT3 (Tyr705) monoclonal antibody, anti-HA monoclonal antibody and SimpleChIP® Enzymatic Chromatin IP Kit (Magnetic Beads) were purchased from Cell Signaling Technology (Danvers, MA, USA). Alexa fluor 488-conjugated anti-mouse IgG antibody, rhodamine (TRITC)-conjugated anti-goat IgG antibody, Alexa fluor 647-conjugated anti-rabbit IgG antibody and secondary HRP-conjugated antibodies were purchased from Jackson

ImmunoResearch Laboratories (West Grove, PA, USA). Propidium iodide was purchased from Invitrogen (San Francisco, CA, USA). MegaCult™-C Collagen and Medium with Lipids was purchased from STEMCELL Technologies (Vancouver, B.C., Canada). Mouse thrombopoietin Elisa kit, anti-Nuclear Pore Complex Proteins antibody and anti-Histone H3 antibody were purchased from Abcam (Cambridge, UK). Nuclear and Cytoplasmic Protein Extraction Kit was purchased from Beyotime Biotech. Inc. (Shanghai, CN). AchE Stain was purchased from Baso Diagnostics Inc. (Zhuhai, Guangdong, CN). Recombinant Mouse Interleukin-3 (IL-3), recombinant Mouse Interleukin-6 (IL-6) and recombinant Mouse Interleukin-11 (IL-11) were purchased from ProSpec (Rehovot, Israel). Recombinant Human Thrombopoietin (TPO) was purchased from 3SBIO, Inc. (Shengyang, Liaoning, CN). All peptides were synthesized by ChinaPeptides Co., Ltd. (Wuhan, Hubei, CN).

Transmission electron microscopy

Washed platelets were fixed in 4% glutaraldehyde at 4℃ for 2 h. After being washed and post-fixed with 2% osmium tetroxide, the platelet pellets were dehydrated. Thin sections were stained with 2% uranyl acetate and lead citrate, and examined under a CM-120 transmission electron microscope (FEI Company, OR, USA).

Next-generation RNA-Seq

Total RNA was extracted using the TRIzol (Invitrogen) and evaluated using the NanoDrop 2000 spectrophotometer (Thermo Scientific). RNA integrity was assessed using the Agilent 2100 Bioanalyzer (Agilent Technologies).

The libraries were constructed using VAHTS Universal V6 RNA-seq Library Prep Kit. Transcriptome sequencing was conducted by OE Biotech Co., Ltd. (Shanghai, China). Briefly, libraries were sequenced on an Illumina Novaseq 6000 platform, and 150 bp paired-end reads were generated. Clean reads were mapped to the reference genome using HISAT.[3] FPKM of each gene was calculated and the read counts of each gene were obtained by HTSeq-count.[4] PCA analysis was performed using R (v3.2.0) to evaluate the biological duplication of samples. Differential expression analysis was performed using the DESeq2. The Gene Ontology (GO) was annotated using the Gene Ontology Database (http://www.geneontology.org/). The processed RNA-Seq data and aligned

reads were deposited in GEO (BioProject: PRJNA1034807).

Liquid chromatography-mass spectrometry (LC-MS)

LC-MS was performed in megakaryocyte lysate Co-IP with anti-PALLD antibody. The mixture of peptides was separated using Zorbax 300SB-C18 peptide trap columns (Agilent Technologies) and tandem mass spectrometry (Thermo Finnigan Q Exactive). Gel digestion, mass spectrometry analysis, and database search were performed at the Core Facility of Basic Medical Sciences, Shanghai Jiao Tong University School of Medicine.

Plasmid construction

Primers were designed based on the PALLD sequence (NM_001166110.2) and STAT3 sequence (NM_001369512.1) from the NCBI website. The target genes were amplified from HEK293T cDNA and then ligated into the pcDNA3.1-Flag or pXJ40-HA vectors, resulting in the generation of Flag-PALLD, Ha-STAT3, and truncated PALLD and STAT3 plasmids.

Protein-protein docking

The crystal structure of PALLD (PDB ID: 2DM2) and STAT3 (PDB ID: 6TLC) were downloaded from the Protein Data Bank. AlphaFold2 predicted structures were referenced to complete the missing PALLD residues. Molecular Operating Environment (MOE) was used to perform protein-protein docking. After the completion of dynamic simulations, the final docking structures were analyzed by the PISA interface server and visualized by PyMOL.

Coimmunoprecipitation (Co-IP)

HEK293T cells were transfected with various plasmids for 48 hours. Total protein was collected using lysis buffer. Protein concentrations were determined by bicinchoninic acid (BCA) assay. Co-IP was performed using anti-Flag M2 Affinity Gel (Sigma) or anti-HA Agarose (Pierce) according to the manufacturer's instructions. All samples were washed with cold TBS, and the precipitated protein was eluted by boiling with loading buffer.

Chromatin Immunoprecipitation (Ch-IP)

Ch-IP assay was performed as described before.[5] Briefly, cells were crosslinked and lysed to release chromatin and fragmented DNA. Anti-PALLD antibody and ChIP-Grade Protein G Magnetic Beads (Cell Signaling Technology) were used to pull down the antibody-protein-DNA complex. After decrosslinking and purification, the enriched DNA was analyzed by PCR or qPCR.

Supplemental figures and figure legends

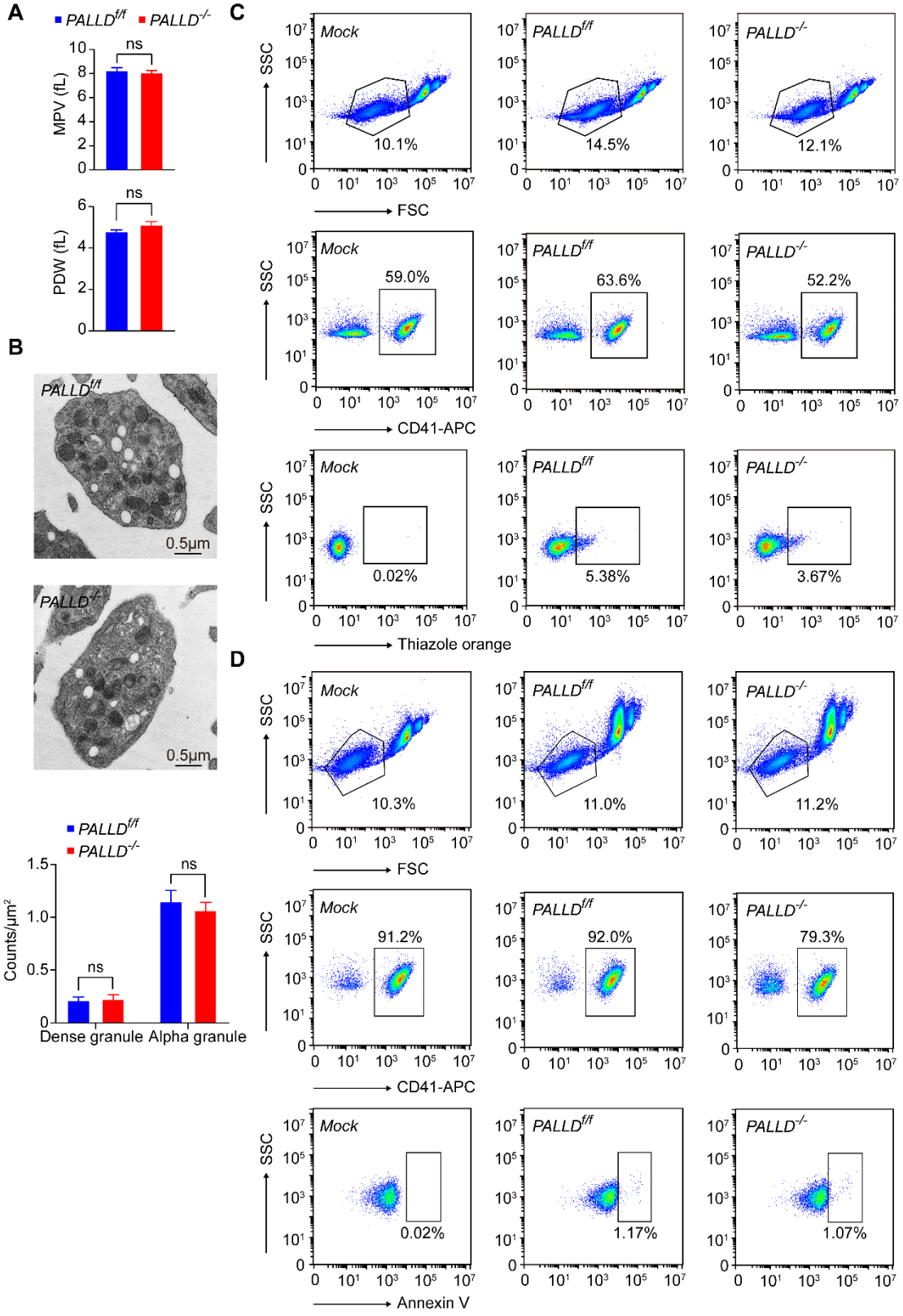

Supplemental Figure 1 (Figure S1)

(A) Mean platelet volume (MPV) and platelet distribution width (PDW) in *PALLD*$^{f/f}$ and *PALLD*$^{-/-}$ mice (n=7; ns, not significant).

(B) Representative images of *PALLD*$^{f/f}$ and *PALLD*$^{-/-}$ platelets under transmission electron microscopy. The scale bars represent 0.5 μm. Quantitative statistics of dense and alpha granules in *PALLD*$^{f/f}$ and *PALLD*$^{-/-}$ platelets (n=10; ns, not significant).

(C) Gating strategy for thiazole orange staining platelets in whole blood from *PALLD*$^{f/f}$ and *PALLD*$^{-/-}$ mice.

(D) Gating strategy for annexin V staining platelets in whole blood from *PALLD*$^{f/f}$ and *PALLD*$^{-/-}$ mice.

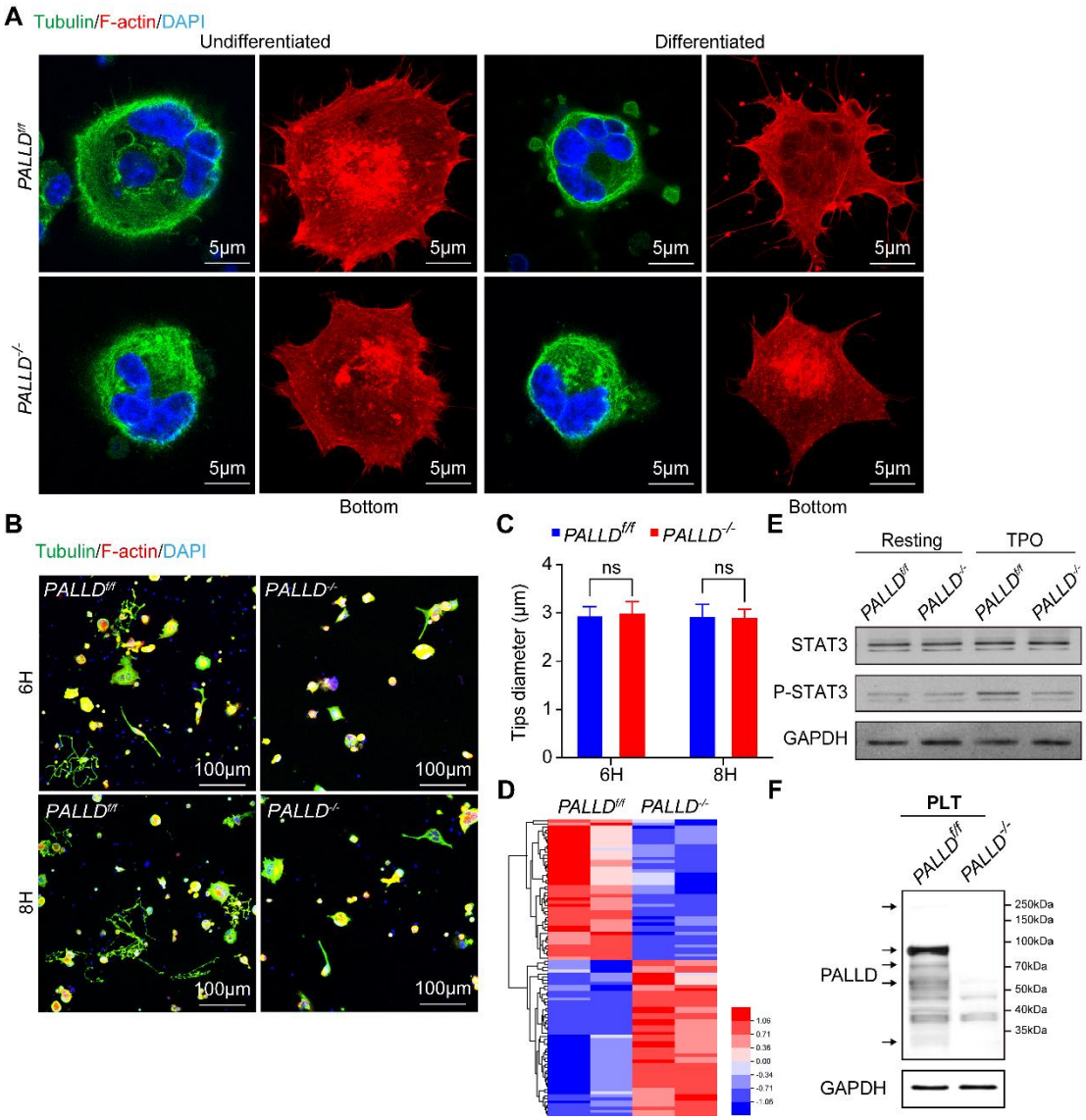

Supplemental Figure 2 (Figure S2)

(A) Immunofluorescence (IF) images of PPF-megakaryocytes derived from the fetal livers of *PALLD*$^{f/f}$ and *PALLD*$^{-/-}$ mice, stained for α-tubulin (Alexa Fluor 488) and F-actin (Rhodamine). The scale bars represent 5 μm.

(B) Representative low-magnification images of PPF-megakaryocytes derived from the fetal livers of *PALLD*$^{f/f}$ and *PALLD*$^{-/-}$ mice, stained for α-tubulin (Alexa Fluor 488) and F-actin (Rhodamine). The scale bars represent 100 μm.

(C) Proplatelet tip diameter in *PALLD*$^{f/f}$ and *PALLD*$^{-/-}$ megakaryocytes (6H, n=5; 8H, n=5).

(D) Heatmap for the clustering of differentially expressed genes in megakaryocytes.

(E) Western blot of the phosphorylation level of STAT3 Y705 in megakaryocytes treated with 25 IU/ml TPO.

(F) Western blot of PALLD expression in platelets of *PALLD*$^{f/f}$ and *PALLD*$^{-/-}$ mice.

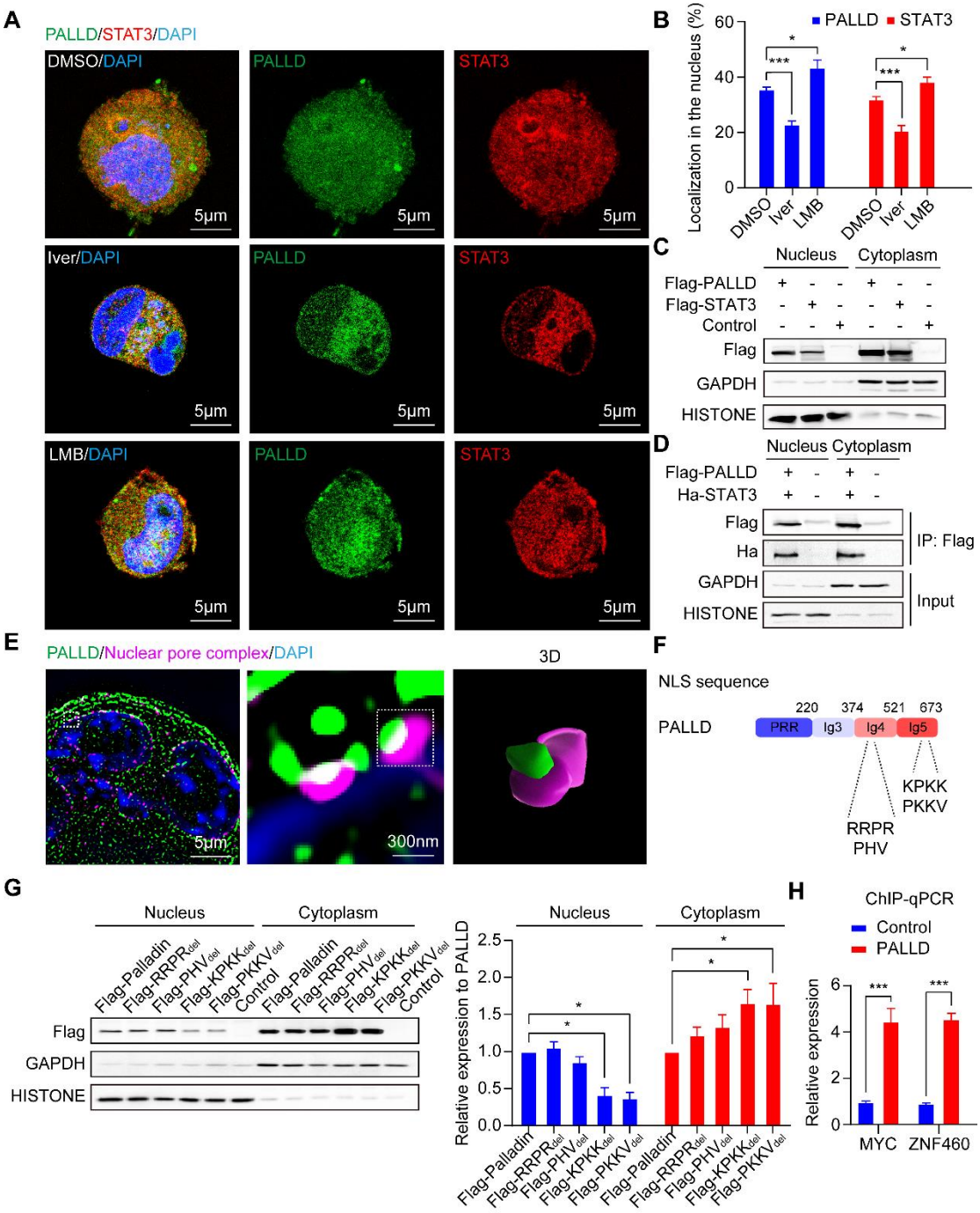

Supplemental Figure 3 (Figure S3)

(A-B) IF images of endogenous PALLD (Alexa Fluor 488) and STAT3 (Rhodamine) in fetal liver-derived megakaryocytes, treated with DMSO, Ivermectin (Iver), and Leptomycin B (LMB). Statistical analysis of PALLD and STAT3 localization is presented (n=5; *P<0.05, ***P<0.001). The scale bars represent 5 μm.

(C) Western blot results of Flag-PALLD or Flag-STAT3 expression in the nuclear and cytoplasmic fractions of transfected HEK293T cells.

(D) Co-IP of isolated nuclear and cytoplasmic proteins from HEK293T cells transfected with Flag-PALLD and Ha-STAT3.

(E) IF images of endogenous PALLD (Alexa Fluor 488) and nuclear pore complexes (Alexa Fluor 647) in megakaryocytes. 3D-volume rendering of PALLD and NPC signals using Imaris software. The scale bars represent 5 μm or 300 nm.

(F) Prediction of nuclear localization signals (NLSs) of PALLD performed by the PSORT.

(G) Western blot analysis of nuclear and cytoplasmic proteins from HEK293T cells transfected with Flag-PALLD lacking the predicted NLSs. Statistical analysis compared the expression levels of NLS-deleted PALLD with normal PALLD in the nucleus and cytoplasm. Statistical analysis of five independent experiments is shown (*$P<0.05$).

(H) QPCR analysis of chromatin immunoprecipitation (Ch-IP) samples from HEK293T cells transfected with Flag-PALLD, utilizing the STAT3-binding promoter sequence as primers. Statistical analysis of four independent experiments is shown (***$P<0.001$).

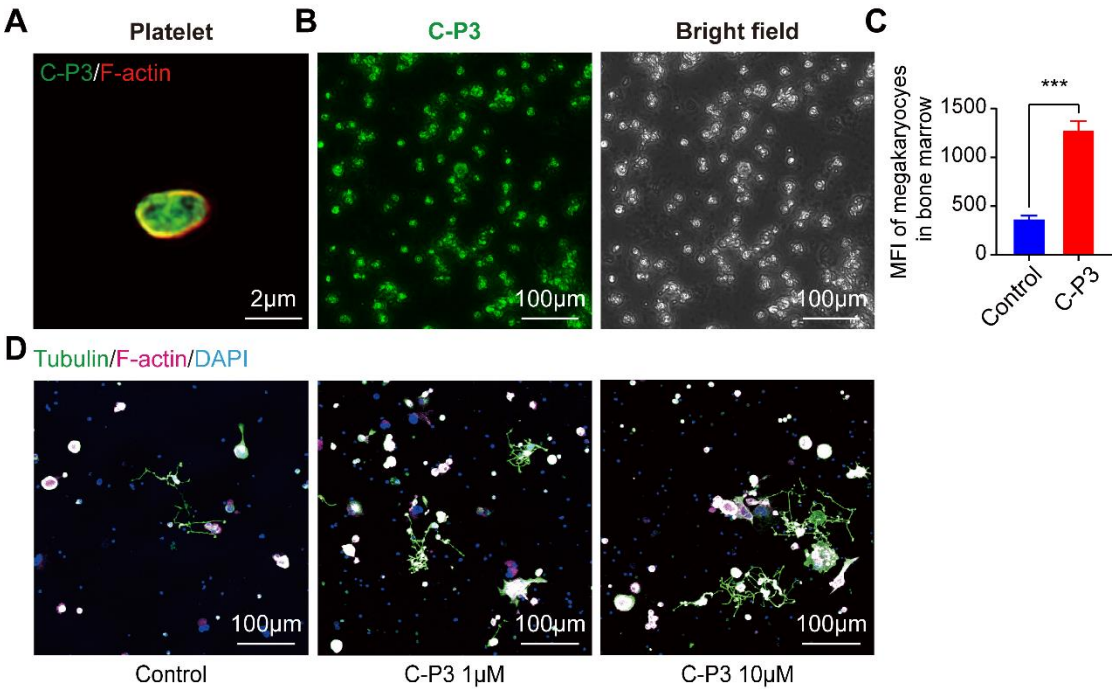

Supplemental Figure 4 (Figure S4)

(A) Representative IF images of platelets treated with FITC-labeled C-P3. The scale bars represent 2 μm.

(B) Representative images of bone marrow smear after bone marrow injection of FITC-labeled C-P3 in mice. The scale bars represent 100 μm.

(C) Mean fluorescence intensity (MFI) of megakaryocytes after bone marrow injection of FITC-labeled C-P3 or 0.9% NaCl in mice (n=4, ***P<0.001).

(D) Representative low-magnification images of fetal liver-derived megakaryocytes stimulated with PBS, or 1 μM and 10 μM C-P3. Stained for α-tubulin (Alexa Fluor 488) and F-actin (Alexa Fluor 647). The scale bars represent 100 μm.

Supplemental Table 1 (Table S1).

List of significantly regulated transcripts related to actin cytoskeleton dynamics.

Gene_id	Expression	FoldChange	P-value	Description
Wipf3	Down	0.218924509	0.017777	WAS/WASL interacting protein family, member 3
Ncald	Down	0.252921713	0.0162624	neurocalcin delta
Fscn1	Down	0.350748923	0.0188354	fascin actin-bundling protein 1
Coro2b	Down	0.38658607	0.0071098	coronin, actin binding protein, 2B

Supplemental Table 2 (Table S2).

List of significantly differentially expressed transcripts.

Gene_id	Expression	FoldChange	P-value	Description
4921536K21Rik	Down	0.029470413	0.0471659	RIKEN cDNA 4921536K21 gene
5430403G16Rik	Up	3.12113323	0.0135198	RIKEN cDNA 5430403G16 gene
6720489N17Rik	Up	2.119412345	0.005745	RIKEN cDNA 6720489N17 gene
AU041133	Up	3.557703218	0.015559	expressed sequence AU041133
AW146154	Up	2.018374121	0.0109815	expressed sequence AW146154
Acsbg1	Up	3.200249097	0.0024462	acyl-CoA synthetase bubblegum family member 1
Acsl6	Up	2.456645331	0.0091594	acyl-CoA synthetase long-chain family member 6
Adamdec1	Down	0.138071133	0.0131127	ADAM-like, decysin 1
Aldob	Up	4.290863573	0.0168796	aldolase B, fructose-bisphosphate
Alpk2	Down	0.24594861	0.0304378	alpha-kinase 2
Ano1	Up	56.37591771	0.009211	anoctamin 1, calcium activated chloride channel
Ano7	Down	0.015578367	0.0054534	anoctamin 7
Apol8	Up	2.261705442	0.0090452	apolipoprotein L 8
Asgr2	Down	0.202217223	0.0141571	asialoglycoprotein receptor 2
Atp9a	Down	0.379531755	0.006009	ATPase, class II, type 9A
B230307C23Rik	Up	2.139218799	0.0005539	RIKEN cDNA B230307C23 gene
B3galnt1	Down	0.459579376	0.0054401	Beta GlcNAc beta 1,3-galactosaminyltransferase, polypeptide 1
Bhlha15	Down	0.468517481	0.0009762	basic helix-loop-helix family, member a15
Bicd1	Up	2.001580012	0.0133114	BICD cargo adaptor 1
Cacna1h	Down	0.345234453	2.39E-09	calcium channel, voltage-dependent, T type, alpha 1H subunit
Cacna1s	Down	0.232007374	0.0001023	calcium channel, voltage-dependent, L type, alpha 1S subunit
Cadm3	Down	0.413712752	0.015913	cell adhesion molecule 3
Ccdc18	Up	2.27128765	0.0019961	coiled-coil domain containing 18
Cd300ld5	Down	0.0923159	0.0023615	CD300 molecule like family member D5
Cd59a	Up	2.031175596	0.0149283	CD59a antigen
Cep290	Up	3.242384053	8.60E-05	centrosomal protein 290
Cetn4	Up	3.138382804	0.0113273	centrin 4
Chst1	Down	0.201619597	1.21E-11	carbohydrate sulfotransferase 1
Cldn7	Down	0.112921016	0.0015498	claudin 7
Cntln	Up	2.016700549	4.13E-05	centlein, centrosomal protein
Coch	Up	18.16729941	0.0146526	cochlin

Col28a1	Up	2.020526789	0.0482233	collagen, type XXVIII, alpha 1
Colca2	Down	0.216483111	0.0003935	COLCA2 homolog
Coro2b	Down	0.38658607	0.0071098	coronin, actin binding protein, 2B
Cpeb3	Down	0.399083508	7.40E-05	cytoplasmic polyadenylation element binding protein 3
Csn3	Down	0.02825396	0.04444	casein kappa
Cxcl3	Up	4.215488079	0.008401	chemokine (C-X-C motif) ligand 3
Cxcl5	Up	3.446174755	0.0023923	chemokine (C-X-C motif) ligand 5
Cyp2b10	Down	0.090751224	0.0005473	cytochrome P450, family 2, subfamily b, polypeptide 10
D3Ertd751e	Up	2.376599844	7.75E-05	DNA segment, Chr 3, ERATO Doi 751, expressed
Derl3	Down	0.282094193	1.29E-07	Der1-like domain family, member 3
Dnm3	Down	0.186658931	0.0122665	dynamin 3
Efcab7	Up	2.384891377	0.0032613	EF-hand calcium binding domain 7
Ehf	Down	0.395467407	0.0117513	ets homologous factor
Epcam	Down	0.281942813	1.33E-06	epithelial cell adhesion molecule
Evc	Down	0.367751952	0.0114762	EvC ciliary complex subunit 1
F8	Up	3.585336831	0.0028301	coagulation factor VIII
Fam177a2	Up	5.76798945	0.002205	family with sequence similarity 177 member A2
Fam78b	Down	0.381849895	0.0496786	family with sequence similarity 78, member B
Fcrl5	Down	0.262818355	0.0012988	Fc receptor-like 5
Fosb	Up	2.17336952	1.32E-07	FBJ osteosarcoma oncogene B
Fosl1	Up	2.2636497	0.0107903	fos-like antigen 1
Fpr3	Down	0.169262714	2.11E-08	formyl peptide receptor 3
Fscn1	Down	0.350748923	0.0188354	fascin actin-bundling protein 1
Fut1	Down	0.30842056	0.0035429	fucosyltransferase 1
Gabra4	Down	0.274690113	0.0430881	gamma-aminobutyric acid (GABA) A receptor, subunit alpha 4
Gbgt1	Down	0.472155493	0.0376127	globoside alpha-1,3-N-acetylgalactosaminyltransferase 1
Gm14295	Up	2.239678618	0.0384968	predicted gene 14295
Gm1604b	Down	0.148767715	0.0029513	predicted gene 1604b
Gm2115	Down	0.015188976	0.0045465	predicted gene 2115
Gm3325	Up	2.454261648	4.29E-05	predicted gene 3325
Gm39469	Up	2.459609458	0.0058742	
Gm39701	Down	0.283576111	0.017259	
Gm45871	Up	2.050081653	0.0187758	predicted gene 45871
Gm46965	Up	2.513454774	0.0114312	
Gm4924	Up	3.89791226	0.0017019	
Gm5111	Up	4.497681186	0.0432071	predicted gene 5111
Gm51425	Up	2.235973714	0.0132717	predicted gene, 51425
Gm7072	Up	2.163085021	0.0005012	predicted gene 7072
Gpr55	Down	0.426431179	0.000151	G protein-coupled receptor 55
H2-M10.1	Down	0.139135025	0.0301976	histocompatibility 2, M region locus 10.1
Hba-a1	Up	2.115042324	1.91E-08	hemoglobin alpha, adult chain 1
Hba-a2	Up	2.224219996	5.43E-10	hemoglobin alpha, adult chain 2
Hbb-bs	Up	2.211920868	1.53E-07	hemoglobin, beta adult s chain
Hepacam2	Down	0.391319762	0.0001738	HEPACAM family member 2
Hmgn5	Up	2.701846976	2.54E-07	high-mobility group nucleosome binding domain 5
Hspa1b	Down	0.467078496	0.0421624	heat shock protein 1B

Ift74	Up	2.040261127	0.0063043	intraflagellar transport 74
Il12b	Down	0.022948436	0.0214607	interleukin 12b
Kcnt1	Up	37.59067702	0.0425164	potassium channel, subfamily T, member 1
Kif20b	Up	2.45576527	0.0267312	kinesin family member 20B
Krt222	Down	0.42695514	0.0212372	keratin 222
LOC101055663	Down	0.09467202	0.003845	
LOC118568705	Down	0.168884689	0.0431426	
Lilr4b	Up	2.113528037	8.36E-07	leukocyte immunoglobulin-like receptor, subfamily B, member 4B
Ly6a	Down	0.426466823	9.61E-06	lymphocyte antigen 6 complex, locus A
Ly6k	Down	0.318986321	0.0112939	lymphocyte antigen 6 complex, locus K
Mecom	Up	2.067623611	0.0487708	MDS1 and EVI1 complex locus
Mfsd4a	Down	0.348224939	0.0126334	major facilitator superfamily domain containing 4A
Msc	Down	0.021547467	0.0361376	musculin
Muc3a	Up	2.027574089	0.0023916	
Nanp	Down	0.227759362	0.0013142	N-acetylneuraminic acid phosphatase
Nbea	Down	0.308420126	0.0058014	neurobeachin
Ncald	Down	0.252921713	0.0162624	neurocalcin delta
Negr1	Down	0.100952369	2.41E-05	neuronal growth regulator 1
Nfkbiz	Up	2.017911653	1.78E-10	nuclear factor of kappa light polypeptide gene enhancer in B cells inhibitor, zeta
Nudt17	Up	3.975427795	0.0494299	nudix (nucleoside diphosphate linked moiety X)-type motif 17
Olfr414	Up	5.888517502	0.030644	olfactory receptor 414
Oosp1	Down	0.353386604	0.0002328	oocyte secreted protein 1
Osm	Up	2.006639369	4.59E-09	oncostatin M
Pgam2	Down	0.228030868	0.0019187	phosphoglycerate mutase 2
Pkhd1l1	Up	2.091841232	0.0021939	polycystic kidney and hepatic disease 1-like 1
Prlr	Down	0.365186526	0.045507	prolactin receptor
Ptn	Up	14.99225129	0.0220518	pleiotrophin
Rbp1	Up	2.092217038	0.0111178	retinol binding protein 1, cellular
Rd3l	Up	20.60192687	0.0397715	retinal degeneration 3-like
Rgs1	Up	2.370495828	4.42E-13	regulator of G-protein signaling 1
Robo1	Down	0.096858929	0.0197843	roundabout guidance receptor 1
Rwdd3	Up	2.668540682	0.0057974	RWD domain containing 3
Sapcd1	Up	2.261970036	0.0281879	suppressor APC domain containing 1
Sdc1	Down	0.385388762	4.58E-09	syndecan 1
Sfrp4	Up	3.22506314	0.0146541	secreted frizzled-related protein 4
Slc13a3	Down	0.47138114	0.0274589	solute carrier family 13 (sodium-dependent dicarboxylate transporter), member 3
Slc25a18	Up	4.983889324	0.0365861	solute carrier family 25 (mitochondrial carrier), member 18
Smim40	Down	0.217189057	0.049222	small integral membrane protein 40
Spag6	Down	0.113432273	0.0021743	sperm associated antigen 6
Spon1	Down	0.115395349	2.94E-16	spondin 1, (f-spondin) extracellular matrix protein
Tcf15	Up	3.538242341	0.043643	transcription factor 15
Tex11	Up	62.06689037	0.0060888	testis expressed gene 11
Tex15	Up	2.237253427	0.00031	testis expressed gene 15
Tex45	Up	3.625797023	0.0259027	testis expressed 45

Tnfrsf17	Down	0.209278987	4.38E-06	tumor necrosis factor receptor superfamily, member 17
Tuba3b	Down	0.029037126	0.0466667	tubulin, alpha 3B
Txndc5	Down	0.471851787	4.30E-07	thioredoxin domain containing 5
Wipf3	Down	0.218924509	0.017777	WAS/WASL interacting protein family, member 3
Zc3h6	Up	2.0176619	0.0002122	zinc finger CCCH type containing 6
Zfp40	Up	2.329059611	0.0017748	zinc finger protein 40
Zfp808	Up	2.1977959	0.0019538	zinc finger protein 808
Zfp820	Up	2.322840335	0.0405505	zinc finger protein 820
Zfp932	Up	2.086325592	4.88E-05	zinc finger protein 932
Zfp942	Up	2.002021322	0.0010809	zinc finger protein 942
Zfp948	Up	2.09951017	0.0046575	zinc finger protein 948
Zfp97	Up	2.178431962	0.0202292	zinc finger protein 97
Zfp970	Up	2.512347693	0.0072403	zinc finger protein 970
Zfp975	Up	2.677253478	0.0075524	zinc finger protein 975
Zfp976	Up	3.830148417	5.89E-05	zinc finger protein 976

Supplemental Table 3 (Table S3).

The information of each pathway in Figure 4C.

GO_id	Term	PopHits	-Log$_{10}$ (P value)	Enrichment_score
GO:0051491	Regulation of cell adhesion	20	2.209933603	16.87719298
GO:0042026	Protein refolding	24	2.054473874	14.06432749
GO:0007259	Receptor signaling pathway via JAK-STAT	32	1.813255551	10.54824561
GO:2001135	Regulation of endocytic recycling	34	1.763105141	9.927760578
GO:0080135	Regulation of cellular response to stress	6	1.74904339	4.018379282
GO:0003374	Dynamin family protein polymerization	35	1.739215251	9.644110276
GO:0032534	Regulation of microvillus assembly	42	1.590356599	8.036758563
GO:0006892	Post-Golgi vesicle-mediated transport	5	1.533432092	33.75438596
GO:0071803	Positive regulation of podosome assembly	48	1.482986373	7.032163743
GO:1903543	Positive regulation of exosomal secretion	7	1.389847724	24.11027569

Reference

1. Hitchcock IS, Kaushansky K. Thrombopoietin from beginning to end. British journal of haematology. Apr 2014;165(2):259-68. doi:10.1111/bjh.12772

2. Tiedt R, Schomber T, Hao-Shen H, Skoda RC. Pf4-Cre transgenic mice allow the generation of lineage-restricted gene knockouts for studying megakaryocyte and platelet function in vivo. Blood. Feb 15 2007;109(4):1503-6. doi:10.1182/blood-2006-04-020362

3. Kim D, Langmead B, Salzberg SL. HISAT: a fast spliced aligner with low memory requirements. Nature methods. Apr 2015;12(4):357-60. doi:10.1038/nmeth.3317

4. Anders S, Pyl PT, Huber W. HTSeq--a Python framework to work with high-throughput sequencing data. Bioinformatics (Oxford, England). Jan 15 2015;31(2):166-9.

doi:10.1093/bioinformatics/btu638

5. Mascanfroni ID, Yeste A, Vieira SM, et al. IL-27 acts on DCs to suppress the T cell response and autoimmunity by inducing expression of the immunoregulatory molecule CD39. Nature immunology. Oct 2013;14(10):1054-63. doi:10.1038/ni.2695